Numerical Simulation of Brash Ice

Rupasingha Arachchige Malith Prasanna

Master Thesis

presented in partial fulfillment
of the requirements for the double degree:
"Advanced Master in Naval Architecture" conferred by University of Liege
"Master of Sciences in Applied Mechanics, specialization in Hydrodynamics,
Energetics and Propulsion" conferred by Ecole Centrale de Nantes

developed at University of Rostock
in the framework of the

"EMSHIP"
Erasmus Mundus Master Course
in "Integrated Advanced Ship Design"

EMJMD 159652 – Grant Agreement 2015-1687

Supervisor :   Prof. Robert Bronsart, University of Rostock

Quentin Hisette, The Hamburg Ship Model Basin

Reviewer :   Prof. Antoine Ducoin, École Centrale de Nantes

Rostock, February 2018

Abstract

Numerical Simulation of Brash Ice is a research project carried out to develop a numerical tool, which is capable of simulating the ships navigating through a brash ice channel. The tool is based on Discrete Element Method and current version is simulating the problem in model scale due to ease of validation. Properties of the ice channel, 3D mesh of structure, propeller characteristics and open water resistance data have to be input to the code. Output consists of numerical results of ice loads on ship, ship velocity and acceleration, pitch and roll angles of ship and graphical output of interaction of ice particles with ship. In order to calibrate the parameters of the code, standard cylinder experiment was simulated and results were compared with the experimental results. Different parameters of the simulation were changed and sensitivity of the results were studied. Graphical output of the simulation was also compared with underwater camera footage. General behaviour of the ice particles were identical in the vicinity of the structure. However the ice loads on structure had discrepancies. Simulation of an Ice Class Tanker was also carried out. Simulation parameters were set to match the actual ship model experiment. Results were compared with experimental values and under water videos. In this case also ice loads tend to be higher than expected. However particle behaviour near hull is acceptable. Cause for high ice loads was identified as deficiency in modelling the behaviour of far field ice particles in current tool. Simulation tend to overestimate the particle motions in far field due to the deficiencies in implemented friction model. (Cundall-Strack Friction). Therefore more work has to be done in order to improve the friction model in simulation environment. Further a more complex Ice-Structure interaction algorithm can improve the quality of results as well. In conclusion the current tool is suitable for obtaining qualitative results on ship navigating in brash ice channel in early design stage. Specially to visualize the ice particle flow around ship hull and identify possible concentration of ice particles especially around appendages.

keywords: brash ice, Discrete Element Method, ice-structure interaction

Contents

List of Figures

List of Tables

Declaration of Authorship

I declare that this thesis and the work presented in it are my own and has been generated by me as the result of my own original research.

Where I have consulted the published work of others, this is always clearly attributed.

Where I have quoted from the work of others, the source is always given. With the exception of such quotations, this thesis is entirely my own work.

I have acknowledged all main sources of help.

Where the thesis is based on work done by myself jointly with others, I have made clear exactly what was done by others and what I have contributed myself.

This thesis contains no material that has been submitted previously, in whole or in part, for the award of any other academic degree or diploma.

I cede copyright of the thesis in favour of the University of Rostock

Date: 15-01-2018   Signature:

Introduction

With the decreases of multi-year ice thickness in arctic region over the past decade, maritime and offshore activities in this region has increased significantly. Ship operators and trade companies are in interest of permanent shipping routes through north passage. Most of the commercial ships passing the arctic will be navigating through the broken ice channels. Therefore, there is a rising need for ice class commercial shipping vessels nowadays [1].

Figure 1: Ship navigating in arctic region

An ice class vessel will need more propulsion power due to the added ice resistance. It has to comply with the classification society rules about installed power on-board. However the existing classification rules are based on empirical formulas and tend to overestimate the power requirement. Installing an overpowered engine will cause the engine to operate in less efficient state. This will cause higher building costs, higher operating cost and most importantly high emissions. Since arctic region is a very sensitive environment, ship emissions can create severe instabilities in nature. Therefore the current industry standard is to perform a brash ice model test to estimate more realistic ice resistance results [2].

However the problem with the model test is, it can be done only in the later stage of design and it is more of a design validation. Hence there is a gap in the current state of the art of designing ice class ships, with regarding the early stage prediction of added resistance due to ice. An early stage estimation of ice resistance will allow designers to develop more efficient hull forms reducing the emissions and operating costs. This can be addressed by a numerical tool which is capable of simulating the Ship-Brash Ice interaction.

Master Thesis

Considering the above requirement, master thesis was carried out to develop a numerical tool based on Discrete Element Method, capable of simulating ship-brash ice interactions. Master thesis topic is:

Numerical Simulation of Brash Ice

The main objectives of the master thesis are, developing a DEM tool to simulate brash ice, calibrating the tool by cylinder experiment and simulating a ship model test.

Implementation

The Hamburg Ship Model Basin has been working on a discrete element method simulation tool to simulate Ship-Ice Ridge interactions over the past few years. Due to the success of the ridge simulation tool, it was used as the initial platform of the new DEM tool for brash ice simulation. Several new modules were added to the code, and some of the existing code sections were modified, so that the tool can simulate both ice ridge and brash ice. Following main topics were identified in the beginning as areas to work on and addressed during the development of tool.

- Numerical Modeling of Brash Ice Particles
- Modeling Ice-Ice Interaction
- Modeling Ice-Structure Interaction
- Generating Brash Ice Channel
- Simulating Cylinder Experiment and Sensitivity Analysis
- Simulating Ship Model Experiment

The tool is written in FORTRAN language and can be compiled and run in both Windows and Linux based systems. In addition it has the capability of parallel computing.

Content Description

Master thesis report consists of four main parts focusing on different aspects of the thesis work. The first part is a general introduction about areas related to the master thesis such as prior art related to brash ice, brash ice numerical simulations and capabilities of the developed tool.

The second part is focused on the code development. It contains description about all the main modules of DEM algorithm in the tool. Since the tool is based on an existing DEM code, more focus was given to describe the modules which were developed under the master thesis for brash ice simulation.

Part three contains the work related to simulation of cylinder experiment and sensitivity analysis. This section describes all the parameters used in the analysis, results of all the simulation and selection of optimum parameters. In addition a comparison of simulation results and experimental results for cylinder experiment is also presented in this section followed by a discussion.

The fourth part explains the work carried out to simulate a ship model in brash ice. It describes, parameters used for the channel generation, model preparation, simulation results and comparison of simulation results with experimental results.

Finally the thesis report is ended with a conclusion on developed tool and possible further developments.

Part I: Overview of Brash Ice-Structure Interaction

1 Brash Ice Introduction

1.1 Natural Formation of Brash Ice and Ice Channel

Brash ice is an accumulation of broken ice rubbles in form of a channel. When a ship passes through level ice, it creates a channel with large broken ice pieces. As other ships pass by the same channel, these ice pieces are re-broken and formed in to a channel filled with ice rubbles. Depending on the environmental conditions, re-breaking process gradually comes to an equilibrium as many ships passing by. Therefore after certain period, particle size and shape reach to an equilibrium distribution. Ice particles in a brash ice channel can be as small as 2 mm to as large as 3 m, and estimated median will be around 1 m. Individual particles approach spheroidal shape due to rounding off of the corners by colliding with passing ships [3].

Figure 2: Brash ice in arctic region

The thickness of the brash ice channel is considerably greater than the surrounding level ice sheet, due to heavy accumulation of ice particles in several layers. A uniform distribution of thickness in the channel can be observed with, considerable thickening near edges similar to side walls. These side walls provide the lateral restraining force preventing spreading of ice layers due to gravity and hydrostatic forces.
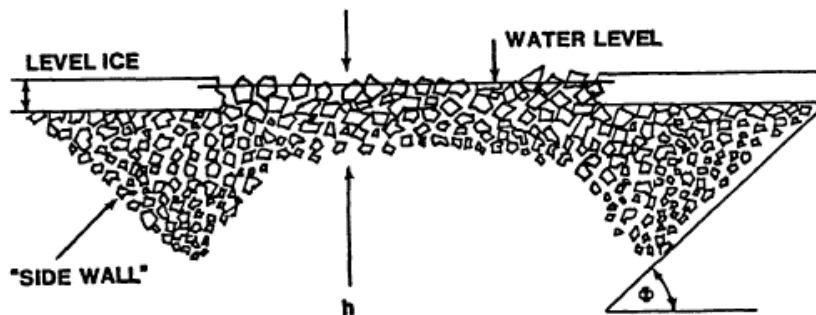
Figure 3: Cross section of a brash ice channel [4]

1.2   Ships Navigating Through Brash Ice

Brash ice is one of the most common form of ice encountered by ice going ships. Ships navigating in ice can be divided in to two groups based on their operations, Ice-Breaking Ships and Ice Class Cargo Vessels. In case of ice-breakers, installed power would be sufficient to navigate through a typical brash ice channel since they are designed to operate in more demanding conditions such as ice breaking and ridge breaking. However in case of commercial Ice Class vessels, good transit performance through ice channel is required by classification authorities. For a commercial Ice Class vessel, added resistance due to ice can be very significant when compared to open water resistance and increases drastically with the thickness of channel. Therefore installed power, onboard has to be increased accordingly. General class rule requirement is that Ice Class commercial vessels should have sufficient installed power to achieve 5 knots in brash ice channel of defined thickness. The ice thickness increases with class notation.

Present Classification Society resistance calculations are based on empirical formulas developed by model tests and full scale experiments. These formulas calculate brash ice resistance based on main dimensions, waterline angle and buttock angle at quarter breadth, bow length and parallel middle body length. Empirical formulas work well on typical size vessels, estimated required power in brash ice, is within acceptable range. However these formulas overestimate the power requirements for large tankers with typical full form hulls. Therefore ship designers often perform a model experiment to prove the transit performance in brash ice channel. There has been number of tanker projects going on, in the ice tank of HSVA over the past years.
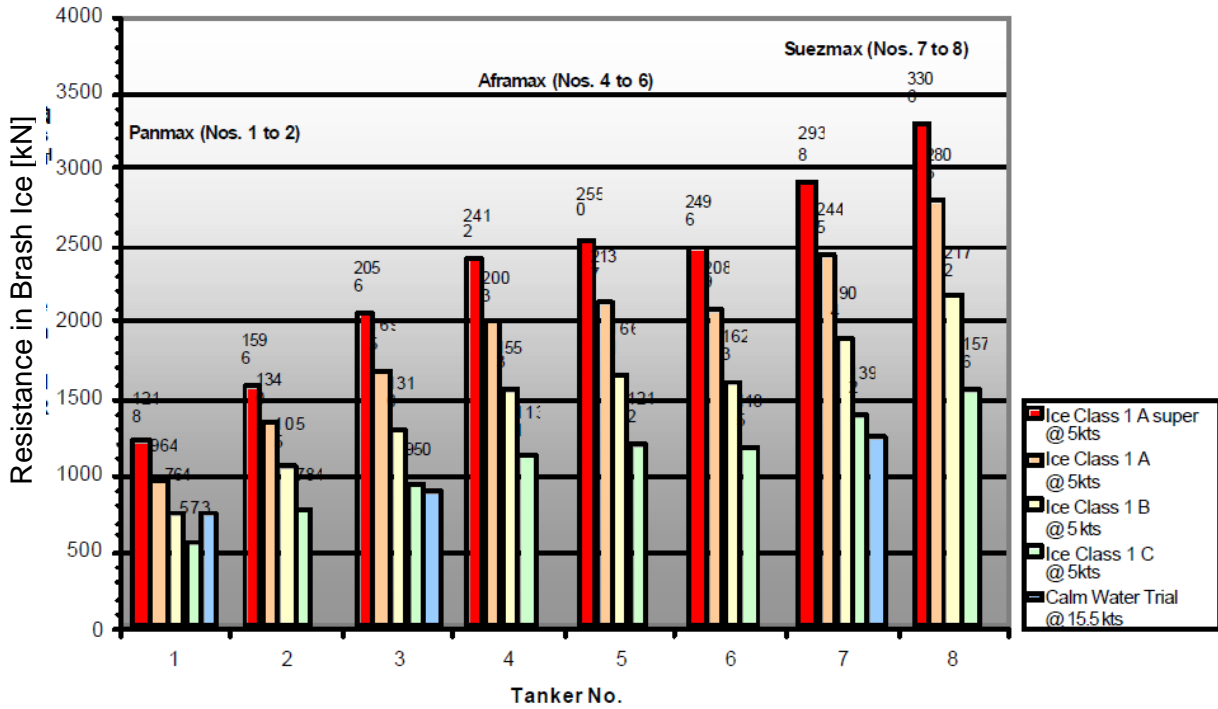
Figure 4: Brash ice resistance calculated from class rules [2]
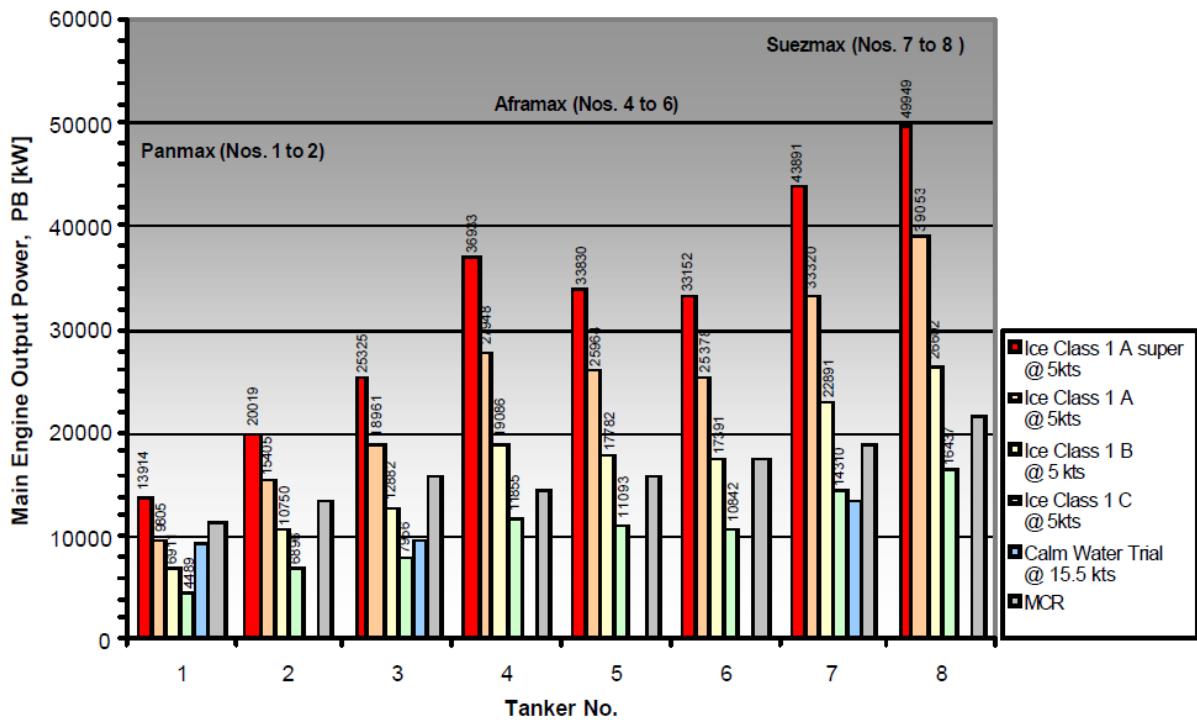
Figure 5: Required main engine power calculated from class rules [2]

Figure 4 and figure 5 show the resistance and powering requirements calculated from class rules for eight tankers of different sizes. It is clear that as the vessel gets larger, ice resistance calculated from class ruled increase drastically which is unrealistic.

1.3 Brash Ice Model Test

Brash ice model test is carried out to prove the transit performance of a ship through a brash ice channel. First the ice channel in towing tank has to be prepared according to specifications. This starts with making a parental ice sheet according to HSVA's standard model ice preparation procedure. After ice sheet reached the desired thickness, a channel is cut in the middle throughout the whole length of the tank. Then, ice sheet in the channel is broken up to small rubbles manually by ice chisels. To obtain the specified ice thickness according to the rules, these rubles are compacted in the channel. Compacting is done in sections by means of a grid from rear end of channel to front end. After creating the channel, brash ice thickness is measured in multiple positions across and 2 m distances over the full length of channel. In addition to that, bending strength of the ice sheet is also measured in four different locations of the surrounding level ice sheet of the channel.

Figure 7: Brash ice preparation

Figure 6: Brash ice channel

Brash ice model tests are performed as towed propulsion tests, varying the propeller load. Model is towed through the channel, while propeller is also pushing the ship. Towing force is measured by the load cell mounted at end of towing rod and, propeller thrust is measured by load cell on line shaft. Propeller RPM changed in four steps during the towing from idling RPM to slightly above maximum installed power. Carriage is towed at speed corresponding to 5

knots in full scale. Carriage and the propeller are synchronized, so that propeller RPM changes automatically in steps, for optimum use of available channel length. Usually two model tests are performed in two different brash ice thicknesses according to the classification requirements. Towed propulsion test is very convenient to find self-propulsion point, since limited length of the channel. Following parameters can be analyzed from the towed propulsion test.

- Total towing resistance in ice
- Developed thrust at self-propulsion
- Delivered power at self-propulsion point
- Propeller efficiency behind the hull in ice
- Thrust deduction factor in ice

Assuming that the thrust deduction factor is constant for a given ship speed and, independent from propeller RPM and thrust, towing force and developed propeller thrust has a linear relationship. Therefore using the linear regression, towing force for zero propeller thrust can be obtained and this value is the total resistance in ice. Then the same regression line can be used to determine the self-propulsion point, where towing force has to be zero. Another regression analysis is done between developed thrust and delivered power from measurements. Then delivered power at self-propulsion point can be obtained by corresponding value of developed thrust.

In general, actual model ice thickness and bending strength can have variations from desired values due to practical reasons of ice making process. Therefore measured values of resistance, thrust and power are adjusted to the target ice conditions. In addition a further adjustment is required for the friction coefficient between ice and model hull, in case there is any deviation. HSVA has developed empirical correction factors for this purpose. Finally model test results are converted to full scale using Froude scaling law. Froude scaling law is working well for medium ice thicknesses. It tends to under estimate resistance for thin ice and over estimate for thick ice. This is taken in to account by means of a correlation factor in the end.

1.3.1 Numerical Simulation of Ice Resistance

Although the model test is the current industry standard to prove ship resistance, numerical simulations has also become very common and widely accepted over the last decade. They are very useful in the early design stage. However availability of numerical tools for simulation of ships going through ice is very limited, due to complex physical models involved. Numerical simulation of Ship-Ice interaction has become a popular research area over the past few years. However research work related to Ship-Brash Ice interaction is limited. This is due to the complex nature of brash ice-water mixture as a medium. In case of simulating behavior of ice floes around ship hull, traditional Computational Fluid Dynamics methods are not very suitable. In this context alternative methods such as Discrete Element Method, Smooth Particle Hydrodynamics and Physical Based Modeling are more applicable.

The major progress so far related to simulation of ships in broken ice is related to simulation of ships in broken ice channels (Lau et al., 2011 [5], Shunying et al., 2012 [6]). Shunying has used a DEM simulation with simplified approach of modeling ice particles and structure floe disks. Lau has used a commercial code DECICE to simulate ships in broken ice fields. The main difference between broken ice channel and brash ice channel is size and packing of the ice particles. Typical particles in a brash ice channel would be 0.1 m to 2.0 m with rounded shapes, while broken ice channel would have larger pieces of level ice sheets.

A DEM simulation of brash ice has been tried (Sorsimo et al., 2014 [7]) with a simple ice model of uniform particles in EDEM commercial DEM software. EDEM is widely used to simulate materials such as soil, gravel and rocks in mining and process industries. Therefore the code is more tuned to work with material like gravel rather ice.

In addition to DEM, Physical Based Modeling Method has also been used to simulate Brash Ice-Structure interactions (Konno et al., 2013 [8]). This method uses Open Dynamics Engine (Physics Engines) which has been developed to simulate various physical systems. Since the code is multipurpose and designed to deal with different scales of problems, it lacks in areas of friction and damping forces approximation methods.

Further, SPH method has been also used to simulate brash ice-structure interactions (Cabrera 2017 [9]). The author has used an open source SPH code and modified the code with new rheological implementations and buoyancy. Modifications were based on available experiments data and work on ice dynamics in HSVA. The tool is capable of simulating

cylinder experiment. However it has not been extended to simulate complex structures such as ship hull. This is due to difficulty of numerical modeling the ship hull with SPH method.

Foundation for this project on Brash Ice-Structure interaction is based on the work of previously developed software for simulation of Ridge Ice Breaking at The Hamburg Ship Model Basin (Hisette et al., 2017 [10]). This software is capable of simulating a ship breaking through ridge ice. Ice Ridge is a special type of ice which has form of wall or line, formed by forced up pressure between two level ice sheets. However the ice particles in a ridge are larger than brash ice and brash ice particles are in a very long channel in contrast to prismatic wall shape of ridge. Results of ridge simulations match the experimental data, showing the capability of DEM in ice-structure interaction simulation.

2   DEM for Ship-Ice Interaction Simulation

2.1   Discrete Element Method Overview

Discrete Element Methods are set of numerical methods, used to calculate the movements and mutual interaction of large number of small particles. This method is based on the assumption that material consist of discrete particles with different shapes and properties. Behavior of these particles are analyzed in Lagrangian Frame by classical rigid body dynamics under interaction forces of contact plasticity, friction, hydrostatic, electrostatic, magnetic, gravitational etc. The Discrete Element Method was introduced as the Distinct Element Method by Cundall in 1979 to solve problems from rock mechanics. Today DEM has extended to EDEM (Extended Discrete Element Method), taking into account thermodynamic effects and CFD and FEM coupling. With the advancement of these coupled simulations and high computational power, DEM became popular in industries such as Agriculture and food handling, Chemical Processing, Civil Engineering, Oil and gas, Mining and Mineral processing, Pharmaceutical, Powder metallurgy; and used to simulate materials such as liquids and solutions (sugar or proteins), bulk materials in storage silos (cereal), granular matter (sand), powders (toner), blocky or jointed rock masses. Although DEM has various applications with different materials, fundamental algorithm is same for most cases and simulations follow the following six step basic algorithm more or less.
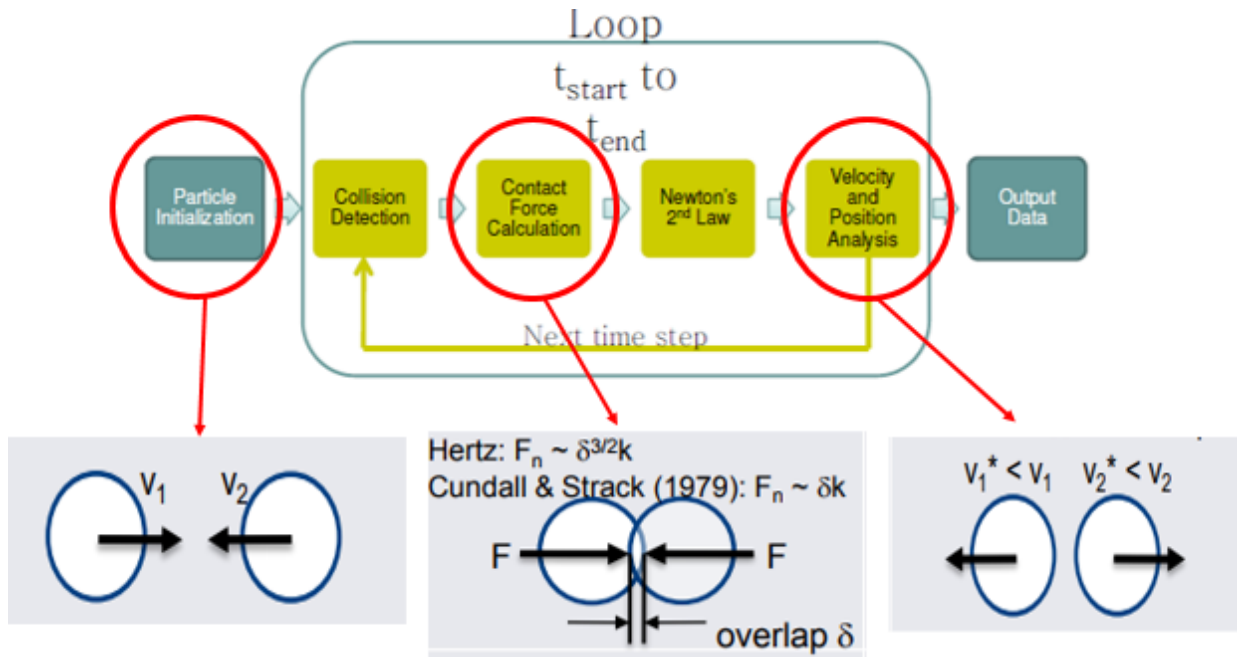
Figure 8: Simple example of DEM simulation – Collision of two spheres [11]

Particle Initialization: DEM simulation starts with initializing the particles and simulation domain. Properties of particles such as shape, initial position, initial velocity, and mechanical properties are defined in this step. In addition properties of simulation domain such as gravitational fields, properties of submerged medium is defined in this step as well. This is one-time operation per simulation and it is outside the main simulation loop.

Collision Detection: In this step, element collisions are identified. Interaction between particles dependent on collision. There are different collision detection methods such as Ray Tracing, Axis Aligned Bounding Boxes, and Direct Collision Detection can be found in literature [12]. One or more of above methods can be used for fast and efficient collision detection.

Contact Forces: Once collision between two particles has identified, interaction can be calculated. According to Hertzian contact law, forces acting between two elements is depending on the amount of overlap volume in the interface. These interaction forces are elastic, damping and friction force. Force are acting on both normal and tangential directions at the interface.

Newton's Second Law: In addition to contact forces there are other forces acting on the elements such as gravity, hydrostatics and hydrodynamics. These forces are calculated in this step. Then Newton's second law is applied on element with sum of all the forces and acceleration calculated.

Velocity and Position: Having calculated the acceleration, velocity and position of elements can be calculated by integrating acceleration function. Numerical integration methods such as Taylor's expansion or Gears Predictor method is suggested in the literature [13].

Time Integration Loop: After calculating the new positions and velocities of the elements, one time step is complete. Since positions of the particles are changed, contacts between elements are also changed in the new time step. Therefore above four steps has to be run iteratively until end of the simulation reached. End condition has to be specifically defined in the simulation.

Data Output: When simulation is competed for all the time steps, results of the simulation are given in this step. This can be numerical and graphical outputs in several file formats. There can be intermediate outputs of the simulation as well, for monitoring purposes.

2.2 Applicability of DEM for Ship-Ice Interaction Simulations

A material should have discrete nature in order to apply DEM. In case of broken ice such as ice floes, brash ice or ridge ice, particles are discrete and behave individually given that there is no ice breaking process or re-freezing. When ship is passing through broken ice, ice particles will move freely due to interaction forces. Ship will also have reaction forces of these interaction and, ship is also free to move individually. Therefore it can be concluded that both ice and ship can be modeled as discrete elements. Then DEM can be used to calculate the interaction forces between particles.

3   Overview of Developed DEM Tool

3.1   Capabilities of Numerical Brash Ice Simulation Tool

The developed code has three options: create brash ice, validate channel properties and ship model test. When initializing the software, user has to select the desired option and inputs has to be given accordingly as well. The code has been developed in model scale for ease of validation. So this can be also considered as a Numerical Ice Tank.

3.1.1 Option 1: Brash Ice Channel Creation

The first module of the software is to generate a brash ice channel according to the given channel parameters. In fact this is the numerical preparation of the environment for brash ice-structure interaction simulation. Channel length, width, brash ice thickness and porosity has to be given as the input parameters. Then the code generates spherical ice particles according to a pre-programed size distribution based on experimental data and locates them in a 3D grid below the waterline. Ice particles will have a random velocity at the beginning as well. Then these particles will float up to free surface due to buoyancy, making up the channel. This method is known as floating up technique. Once the channel is generated, it can be saved and can be used for ship model tests later.
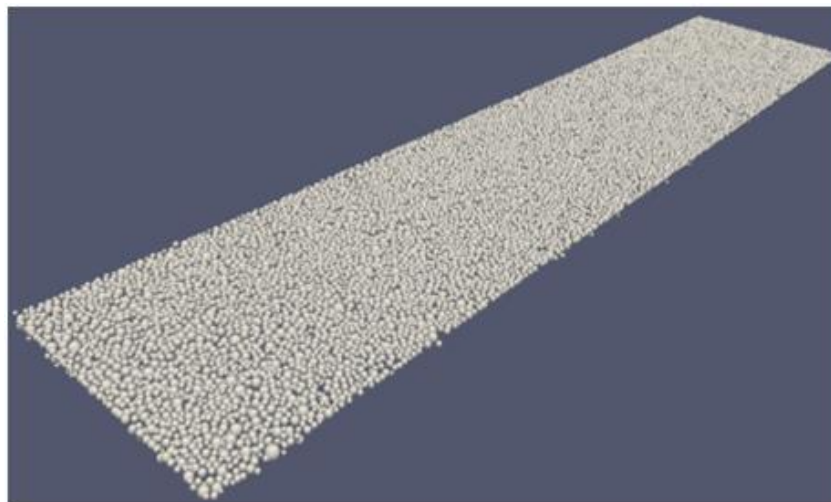
Figure 9: Brash ice channel

3.1.2 Option 2: Validation of Channel Properties – The Cylinder Experiment

In the second part of the software a standard cylinder experiment is simulated on a channel. Cylinder experiment is a reference test used in HSVA ice tank to compare the properties of different ice channels. Therefore it was also implemented in the code to compare and standardise channel data. In this experiment a 0.2 m diameter cylinder is towed through brash ice and forces are measured. Generally HSVA has reference results for this test which can be compared with experimental measurements. Therefore this test can be used to calibrate the simulation results. Input for this part of the code would be channel data from the first part and a 3-D model of the cylinder.
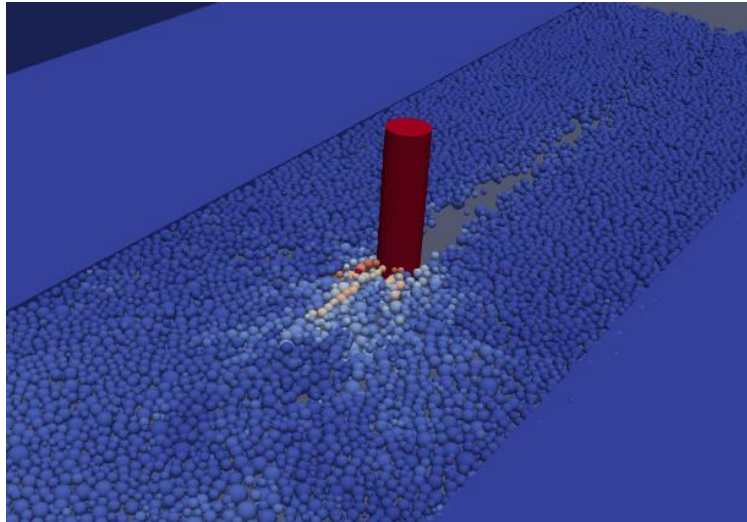
Figure 10: Cylinder experiment-above water view

3.1.3   Option 3: Ship Model Test

In the third part a self-propulsion model test of a ship in brash ice is simulated. A 3-D model of the ship, channel data, propeller curve and open water resistance of the model have to be input in to software. Evolution of ice forces and propeller thrust can be obtained after the simulation and can be converted to full scale for engine selections. In addition graphical output of the simulation can be used to visualize the ice particle flow around hull. This can be used to check possible ice interaction for propeller and to check whether there is any risk of clogging of ice particles around appendages. Early design stage identification of possible propeller ice interactions and ice particle clogging is very important since these problems might lead to major design modifications.
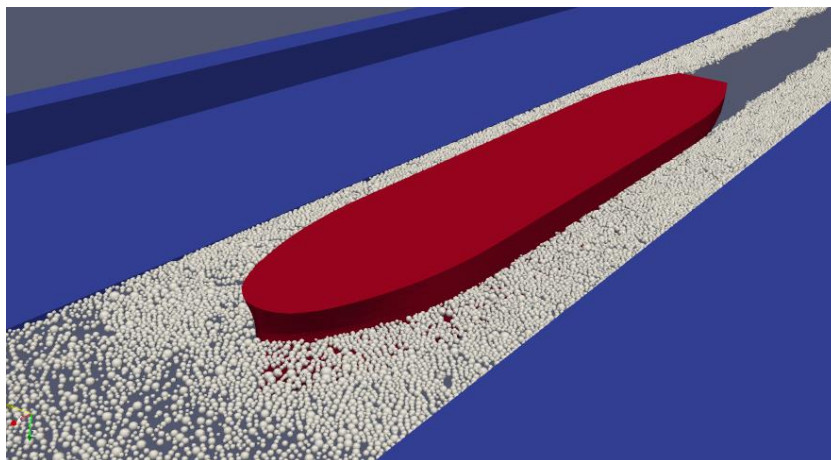
Figure 11: Ship model test

Part II: Dem Algorithm in Developed Tool

4   DEM Algorithm in Numerical Brash Ice Simulation Tool

Basic principle of a DEM was introduced in the section 2.1. However to simulate ship-brash ice interactions, a more complex algorithm is required. The DEM algorithm in the developed software is given below. This is an extension of basic DEM principle with additional steps to calculate ship dynamics and provide graphical outputs.
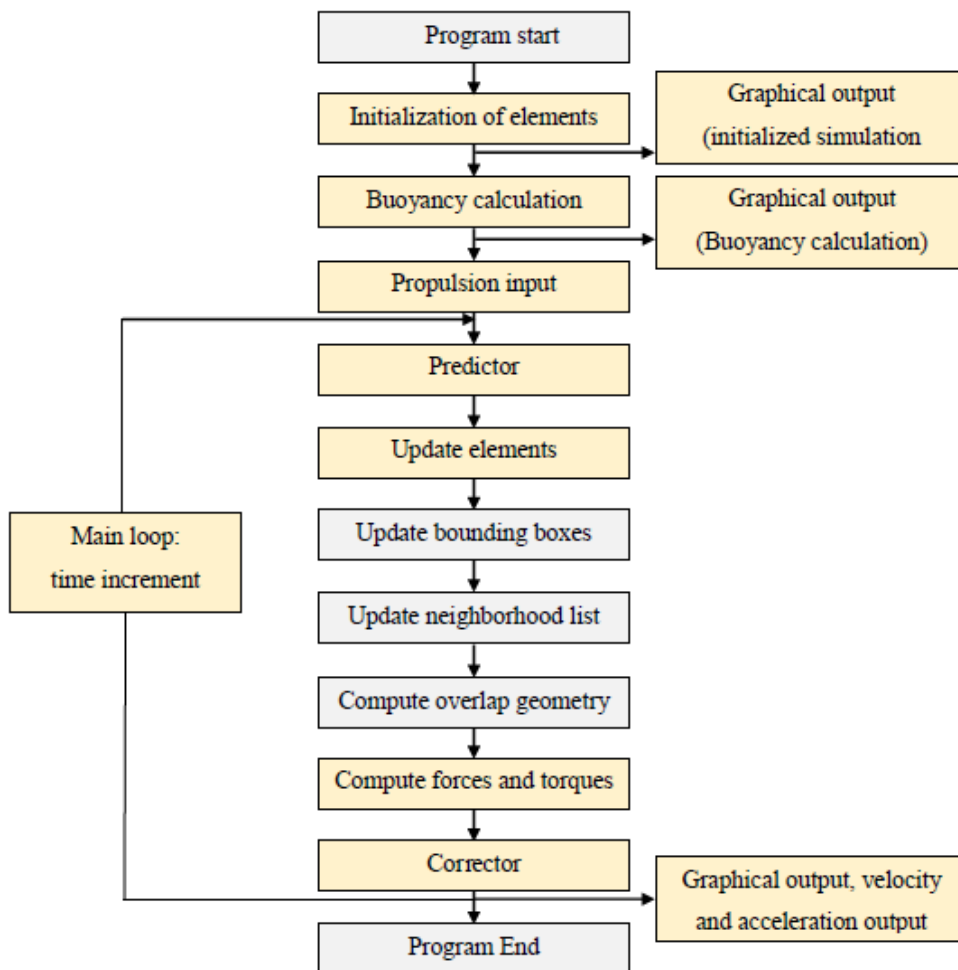
Figure 12: DEM algorithm in developed tool [14]

Function of each step and more details will be discussed in the next sections according to the order in algorithm.

5   Initialization of Elements

This is the first step of the simulation and it has two separate modes for brash ice channel generation and cylinder experiment or ship model test. Actual modelling of ice particles will be done only in channel generation. For cylinder experiment or ship model test, definition of ice particles will be imported from a previously completed simulation of channel generation. However defining the structure elements of cylinder experiment or ship model test will be done in these steps respectively.

5.1   Numerical Modelling of Brash Ice

As the first step of program, ice particles have to be modelled numerically. Since ice is the medium where ship is sailing, accuracy of end results are heavily dependent on this step. Therefore an experimental approach was used to derive a good numerical model of brash ice and this is one of the main uniqueness of the proposed software solution.

Since the simulation should have very large number of ice particles to model brash ice, simple geometric shape of ice would make the software faster. Therefore brash ice particles were modelled as spheres. Hence any particle can be defined with two parameters; position vector of the centre and the radius. This assumption is rational since ice particles in an actual sea ice channel also have more roundish shape which can be seen in figure 2. Ice particles in a brash ice channel tend to get their edges rounded off by passing ships. However using of spherical particles is not much encouraged in DEM simulation of granular material due to rolling effect of spherical particles [13]. In other words if we pour a typical granular material on to a plane, they tend to form a pile, mainly due to friction and interlocking of particles. Although this is not the case of spheres. However if spheres have very high friction coefficient they can also get piled up. In the case of brash ice, it is experimentally proven that brash ice has very high friction angles (40°-50°) which leads to high friction coefficients [15]. Therefore using spherical particles with high friction angles can be justified.

As the next step, size of the ice particles has to be defined. Since the Newton's Laws are applied in the DEM method, it is important to have the correct mass of the ice particles. From previous ship scale measurements, it was shown that ice particle size distributed in a lognormal distribution [3].
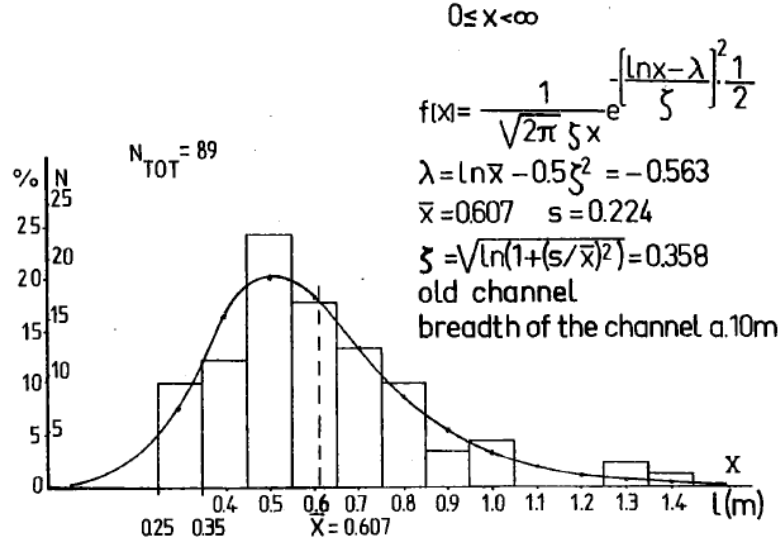
Figure 13: Particle size distribution in ship scale [3]

However this has to be converted to model scale. Taking the advantage of Ice Tank facility in HSVA, a small experiment was carried out and measured the weight of brash ice particles with different ice samples. Then volume of each particle was calculated with measured ice density and from volume a radius was calculated for a spherical particle having the same weight. Then parameters of lognormal distribution (mean and standard deviation) was calculated from this data. Following results were obtained from the calculation

Table 1: Ice particle size statistical data

Mean: radius	0.01740245 m
SD: radius	0.00545217 m
Mean: ln(radius)	-4.09421345
SD : ln(radius)	0.2870471

These results were implemented on a random lognormal generator code [16]. So when generating ice particles, software calls this function and generate random radius values.

$$particle\ radius = e^{gen\_norm(-4.0942, 0.2870)} \qquad (1)$$

Here the gen_norm function generates a random number from a normal distribution of given mean and standard deviation. Particle radius is in natural exponential of generated random number. A particle sample similar to experiment, was generated by the code and particle size was compared. Distributions of experiment and simulation particle size, are matching.
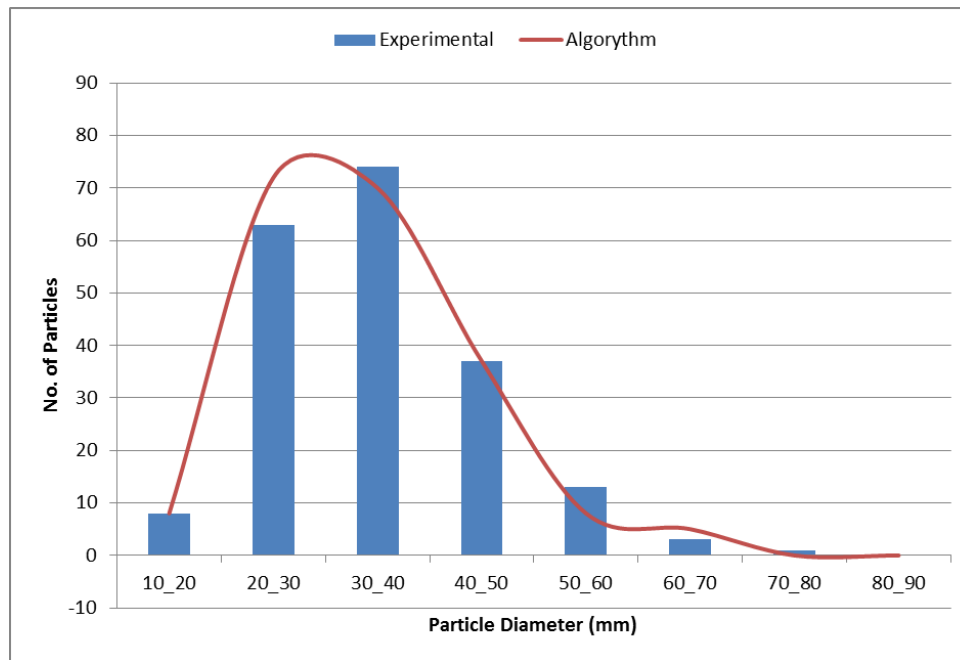
Figure 14: Particle size comparison between simulation and experiment

As the next step, code calculates the number of ice particles required in the channel based on ice volume. Generally a brash ice channel in ice tank experiment, is defined by the length, width, brash ice thickness and porosity. In this case porosity means the ratio of non-ice volume to total volume. Same parameters were used as input of the software. When user input the desired channel parameters, software calculates the total ice volume in the experimental channel.

$$Ice\ Volume = length \times width \times brash\ ice\ thickness \times (1 - porosity) \quad (2)$$

To get the same channel properties as experiment, total volume of ice particles has to be same for both simulation and experiment. Therefore software generates ice particles until total ice particle volume reach the experimental value.

Then these particles has to be positioned in the simulation domain uniformly, to get same properties throughout the channel. In addition location of the particles has to be random and particles have to form a pile. To achieve this, the floating up technique is used in the simulation. Therefore ice particles are assigned a position vector, so that they form a 3D array in the underwater region. Random initial velocity in X, Y and Z direction is assigned as well. In addition to above density, friction co-efficient and Young's modules of ice particles are also defined.
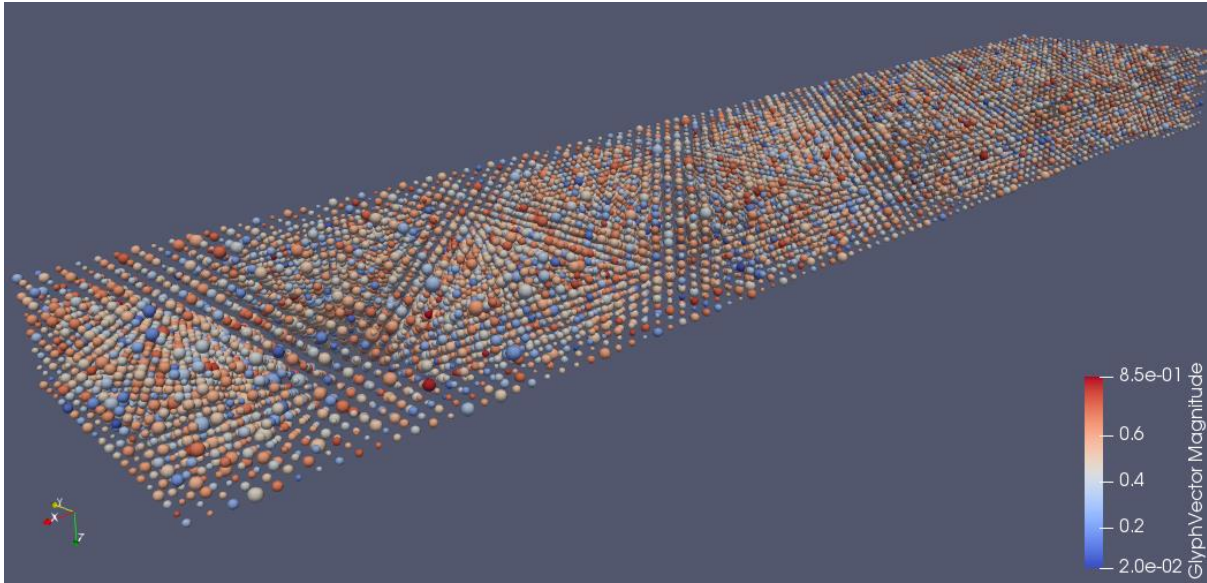
Figure 15: Initial grid of ice particles-particle color represent the random initial velocity

Figure shows the, initial array of ice particles in channel generation. Particles will float up to free surface in channel generation during the simulation. As explained earlier, for cylinder experiment and ship model experiment, particle definitions are directly read from output files of channel generation.

5.2   Discrete Element Modelling of Structure

Numerical modelling of the structure elements is also done on this part of the code. A triangulated surface mesh is used in the tool to model the structure elements. Surface boundary of the structure is made of triangles and, coordinated and topological index of each of these triangle are input to the tool as an .obj file.

```
# Rhino

v 0.125 0 0.166667
v 0.125 0 0.2
v 0.125 0 0.233333     3D coordinates of vertices
v 0.125 0 0.266667
v 0.125 0 0.3

f 622 560 559
f 560 498 497
f 498 436 435          Index of vertices forming
f 436 374 373          face
f 374 343 342
```

Figure 16: Sample .obj file-rows starting

In the example rows starting with v consist data of coordinates of the vertices of triangles. Rows starting f gives the topology of above vertices to form triangles. These information are stored in the code using two arrays *vert_coord* and *face_vertex_table*.

VERT_COORD

vertex index: $1 \rightarrow 4$

V_{1x}	V_{2x}	V_{3x}	V_{4x}
V_{1y}	V_{2y}	V_{3y}	V_{4y}
V_{1z}	V_{2z}	V_{3z}	V_{4z}

Figure 18: Data structure for coordinates of vertices

FACE_VERTEX_TABLE

face index: $1 \rightarrow 4$

1	1	1	2
2	3	4	4
3	4	2	3

Figure 17: Data structure for face index

When code needs to referrer to specific triangulated face of structure, first relevant vertex indexes are obtained from face_vertex_table according to face_index and then to the coordinates from vert_cord.
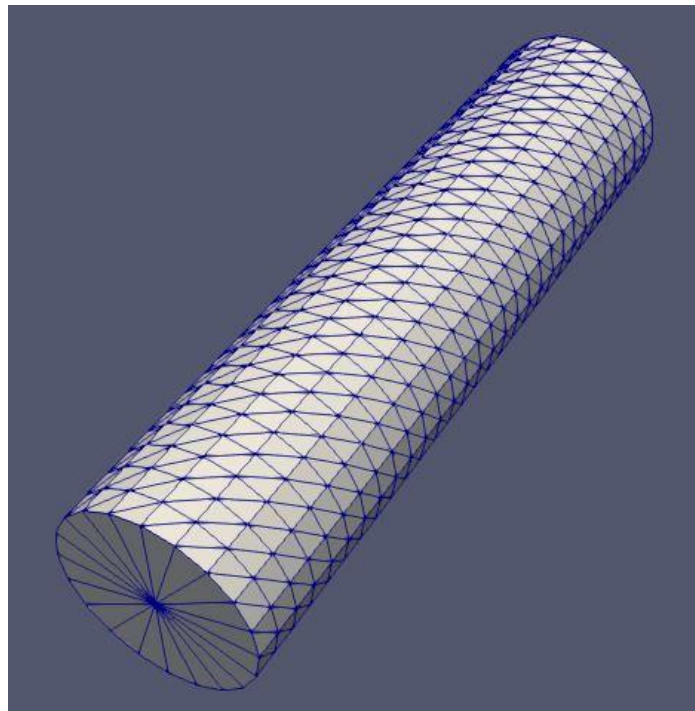
Figure 19: Triangulated surface mesh of cylinder

The overlap computation algorithm used in the developed tool only works with convex shapes. However modern ship hulls have highly non-convex shapes, especially in the bow and stern. This non-convex parts can create numerical leakage in structure boundary causing ice particles to penetrate in to ship. Therefore importing ship hull as a single element directly into simulation, is not possible. This problem can be handled by treating non-convex bodies as a

composites of convex bodies. Ship hull is divided in to several convex bodies in advance and input into simulation as multiple elements. A standard CAD package supporting .obj file format can be used for this, and .obj files are created for each sub body. To avoid conflicts of the sub bodies, all points and topological data in mesh files have to be given with respect to the centre of gravity of ship. In addition to point data of sub-bodies, centre of gravity of the sub-bodies are also input in another file. Centre of gravity of sub-bodies are required to calculate overlap volume, and to correct rotation of ship hull elements in later stages. In addition to handling numerical leakages, sub-elements in structure is also making the overlap detection faster. This will be explained in the end of ice structure overlap calculation section.

5.3   Buoyancy Calculation and Propulsion Input

As the ship passes through ice channel, ice forces start to act on hull changing ships draft, trim and heel. Therefore, hydrostatics has to be calculated in each time step. However, hydrostatics calculation of a complex ship geometry requires large amount of computations. Running them inside the main loop for each time step will slow down the main loop. Therefore hydrostatics and propulsion data are calculated before initiation of main loop. In case of hydrostatics, it requires displacement, centre of buoyancy and restoring moments of ship for changes in displacement, roll and pitch. In hydrostatics calculation section, a 3-dimensional data array is generated. First ship is divided in to certain number of cross sections along the length. Then underwater section area is calculated for all the sections using gift wrapping algorithm. Finally total underwater volume can be calculated using the Simpson's rule on section areas. This procedure is followed on all the draft, trim and heel cases to generate the buoyancy table.
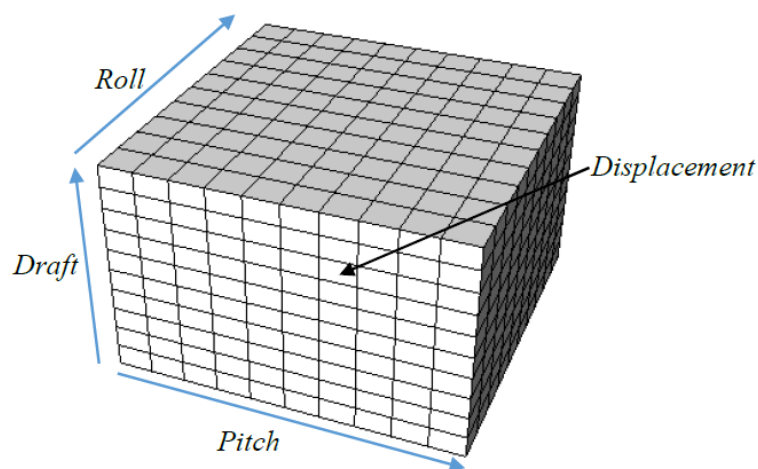
Figure 20:3D data array for hydrostatic data [14]

In next step data from propeller open water test are input to the code in tabular form to calculate propeller thrust. A table of thrust coefficients against advance ratios is used.

After initializing elements and calculations, main loop starts.

6 Predictor: Time Integration of Dynamics Equations

In order to get the velocity and position of ship over the time, position vector equations has to be time integrated. Downwind implicit scheme is used in the code for time integration of dynamics equations. Gear's predictor algorithm is used to solve the equations numerically. This method has two steps for calculating time integration value. First, desired physical quantity is estimated in next time step using numerical scheme such as Taylor's expansion. This step is called predictor step. However due update of contacts after the predictor, there will be an error in predicted value. This error is calculated using Gear's method and then plugged to predicted value accordingly to compensate the error in corrector step of the algorithm [17].

To solve the dynamics of a particle it only requires position vector (r) and quaternion (q).

Using second order Taylors expansion on position vector

$$r_p^{t+\delta t} = r^t + \dot{r}^t dt + \frac{1}{2}\ddot{r}^t dt^2 \tag{3}$$

$$\dot{r}_p^{t+\delta t} = \dot{r}^t + \ddot{r}^t dt \tag{4}$$

Here $t + \delta t$ denotes that position vector is after δt time from current time, t denotes current time step and p denotes it is predicted value. These equations will be same for quaternions as well.

7 Overlap Calculation

In DEM scheme, interaction forces acting between two elements depend on the amount of overlap volume in interface. In order to calculate the degree of interaction between ice particles, first it is required to detect the possible overlaps. Detection of possible overlapping particles is done by two stage sorting algorithm. In first instance an Axis Aligned Bounding Box method is used to detect the possible overlaps. This is done with both ice and structure elements.

First a bounding box is created around the element, with maximum dimensions of the element. Then possible overlapping cases can be detected by sweep and prune sorting algorithm in X, Y and Z directions. If there is no overlap between axis aligned bounding boxes, there is no possibility to have an overlap between these two elements. Therefore this is a fast method to identify elements which are not overlapping. If there is an overlap of bounding boxes, two elements are entered to an array of possible overlap pairs.
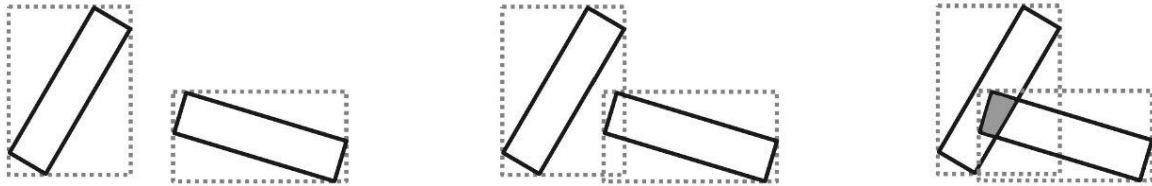
Figure 21: Bounding box overlap [17]

Figure 21 illustrates that, overlapping bounding boxes does not prove that two elements are in contact. Therefore these possible contact pairs have to be confirmed using a more extensive contact detection algorithm. Since simulation consist of both spherical elements and polyhedron elements, two distinct contact detection algorithms are used.

7.1   Ice-Ice Overlap

Since ice particles are spherical, confirming the overlap is very straightforward. If distance between centres of two spheres is less than the sum of radii, then two spheres are overlapping. This check is done for all the ice elements entries in bounding box overlap list.
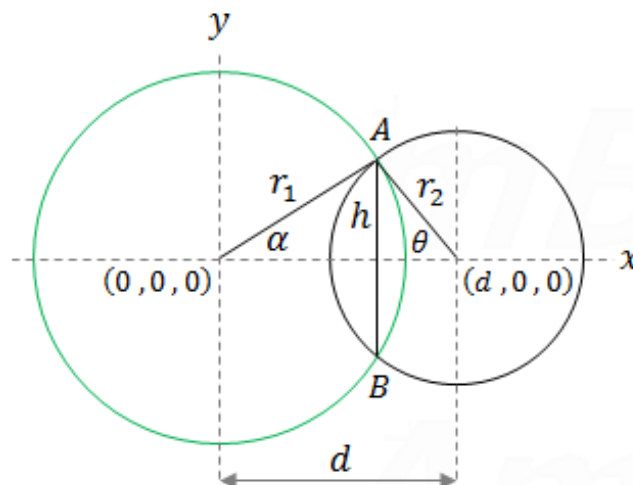
Figure 22: Two overlapping spheres [18]

Overlap Condition;

$$d < r_1 + r_2 \tag{5}$$

Where in 3D space;

$$d = \sqrt{(x_2 - x_1)^2 + (y_2 - y_1)^2 + (z_2 - z_1)^2} \tag{6}$$

After confirming two overlapping ice elements, overlap properties are calculated using analytical formulas. Overlap volume consist of two spherical caps. Therefore properties of spherical caps are calculated separately and then summed together.

From cosine law

$$\alpha = cos^{-1}(\frac{r_1^2 + d^2 - r_2^2}{2r_1 d})$$

$$\theta = cos^{-1}(\frac{r_2^2 + d^2 - r_1^2}{2r_2 d}) \tag{7}$$

Overlap volume consist of two spherical caps. Height of the spherical caps can be found;

$$h_1 = r_1(1 - cos\alpha)$$

$$h_2 = r_2(1 - cos\theta) \tag{8}$$

Therefore Overlap Volume;

$$V_1 = \frac{\pi h_1^2}{3}(3r_1 - h_1)$$

$$V_2 = \frac{\pi h_2^2}{3}(3r_2 - h_2) \tag{9}$$

Total overlap volume would be;

$$Overlap\ Volume = V_1 + V_2 \tag{10}$$

Then we can find intersection circle radius by;

$$h = r_1 sin\alpha = \frac{\sqrt{r_1^2 d^2 - (r_1^2 + d^2 - r_2^2)^2}}{2d} \tag{11}$$

Overlap area is the area of intersection circle;

$$Overlap\ Area = \pi h^2 \tag{12}$$

As the next step centroid of overlap volume has to be calculated. To ease the calculations a reference coordinate system is used with origin on center of 1st sphere with global coordinates x, y, z directions. Center of gravity of two spherical caps are calculated separately and then combined.

$$CG_1 = \frac{3(2r_1 - h_1)^2}{4(3r_1 - h_1)} \tag{13}$$

Above formula gives the center of gravity of spherical cap with respect to the center of sphere. Therefore to be on the reference coordinate system formula for second spherical cap;

$$CG_2 = d - \frac{3(2r_2 - h_2)^2}{4(3r_2 - h_2)} \tag{14}$$

Therefore distance to the centroid of overlap volume;

$$CG = \frac{V_1 CG_1 + V_2 CG_2}{V_1 + V_2} \tag{15}$$

This distance is along the line connecting two centers. Therefore coordinates of centroid of overlap volume on global coordinate system can be calculated as;

$$Overlap\ Centroid = [x_1 + CG \times x_{unit}, y_1 + CG \times y_{unit}, z_1 + CG \times z_{unit}] \tag{16}$$

$$center\ of\ sphere_1 = [x_1, y_1, z_1] \quad center\ of\ sphere_2 = [x_2, y_2, z_2]$$

$$x_{unit} = \frac{x_2 - x_1}{d} \quad y_{unit} = \frac{y_2 - y_1}{d} \quad z_{unit} = \frac{z_2 - z_1}{d}$$

Finally force direction of normal reaction between two spheres has to be calculated. In this case also 1st sphere was taken as the reference. Force direction is given by unit normal vector to overlap surface. Which is the normal vector between two centers of spheres. However normal reaction force on sphere 1 has to be towards the sphere 1, to separate colliding spheres. Therefore;

$$Force\ Direction = -[x_{unit}, y_{unit}, z_{unit}] \tag{17}$$

7.2   Ice-Structure Contact Detection

In this case structure element is a ship section with triangular surface mesh and ice particle is spherical element. Therefore a sphere triangle overlap detection algorithm based on separation axis principle is used to confirm ice structure overlaps.

7.2.1   Separation Axis Principle

"If two convex objects, C1 and C2, are not intersecting there must exist a pair of points P1 and P2, one from each object, such that no other pair of points are closer than these points. Given such a pair, we can insert a separating plane between P1 and P2, with normal P2 - P1. We call P2 - P1 a separating axis" [19]. In fact the principle describes the condition for no overlap.

Therefore to prove two objects are not overlapping, separation points has to be identified. However it is not practical to test all the points on two objects, since there are infinite number of possibilities. Therefore we classify all the points in to finite number of features, so that they share the same test for separation. After that, candidate axes has to be formed for all future pairs from two objects, to identify separation.

For a triangle there are three kinds of features which has to be tested. They are three vertices, three edges and one face. And for a sphere there is only one feature, which is spherical surface. However, there are infinite number of points on surface. So the testing feature is the point on the sphere surface which is closest to each given triangle feature.

Define Triangle T by vertices A, B and C, Sphere S by centre P and radius r. Then following axes have to be checked for separation.

- Normal axis to the triangle plane
- Axis through A and P
- Axis through B and P
- Axis through C and P
- Axis perpendicular to AB and through P
- Axis perpendicular to AC and through P
- Axis perpendicular to BC and through P

Triangle plane can be divided in to seven regions, according to the relative position of sphere and triangle, based on last six cases of the list. In plane separation case sphere has not in contact with triangle plane.
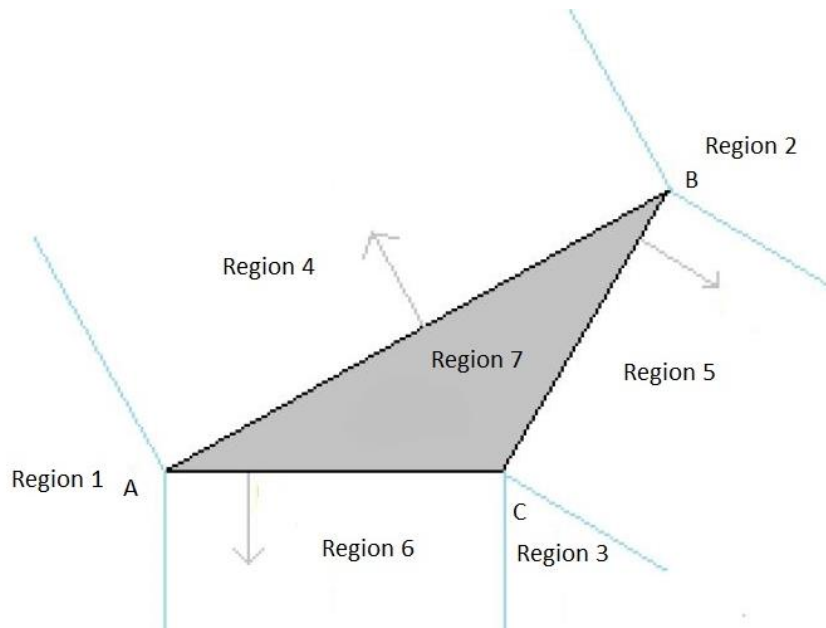
Figure 23: Different regions in separation axis principle

For the calculations in this section A, B and C are the position vectors of the vertices of triangle with respective to centre of the sphere P and r is the radius of sphere, a scalar. All the symbols are in vector mechanics notation (dot product, cross product and absolute in their usual meanings).

Separation axis through triangle plane

There is no intersection of sphere and triangle if, sphere is located further away from the plane of triangle than radius. This can be proved by;

Normal vector to the triangle plane and unit normal vector.

$$V = (B - A) \times (C - A)$$

$$N = \frac{V}{|V|}$$

(18)

Then distance between sphere centre and triangle plane;

$$d = |A.N|$$

(19)

$$If\ d > r\ then\ sphere\ and\ triangle\ are\ separated$$

Separation axis through a vertex of a triangle

For the vertex A of the triangle

Distance between sphere centre and vertex A;

$$d = |A|$$

The normal axis to the plane through A, with normal (A-P) is separation axis if;

$$d > r$$

Points B and C are on the opposite side of the plane with respect to P

$$(B - A).A > 0$$

$$(C - A).A > 0$$

If all above conditions are satisfied; there is no intersection between sphere and triangle. Sphere is located in the region 1 of figure 23. Same procedure has to be followed to check the separation with respect to vertices B and C. If true the sphere is on region 2 or 3 in the figure with respectively.

Separation axis through an edge of a triangle

In this case a separation plane through edge AB, with normal through P and perpendicular to AB is calculated. As the first step projection of P on line AB, point Q is calculated. Q is actually the projection on to triangle plane and must, by construction fall on to AB.

$$AB = (B - A)$$

$$t = \frac{(P - A).AB}{AB.AB} \tag{20}$$

$$Q = A + t.AB$$

Then distance the Q from P is calculated

$$d = |Q|$$

The normal axis to the plane through AB, with normal through P and perpendicular to AB is separation axis if;

$$d > r$$

Point C is on the opposite side of the plane with respect to P

$$(P - Q).(C - Q) < 0$$

If above two conditions are satisfied there is no intersection. Sphere is in the region 4 of figure 23. Same procedure can be followed to check the separation with respect to edges AC and BC. Then sphere is on region 5 or 6 respectively.

After checking all the seven axes and none of them separate the sphere from tringle, then we can conclude that they are overlapping. Given that ice particle diameters are relatively small when compared to structure mesh triangles, and time step of simulation is sufficiently small, it can be seen in figure 24 that there are three possible overlap cases between a sphere and triangle: overlap with vertex of a triangle, overlap with edge of a triangle, overlap with face inside the triangle. Each of these cases has to be identified and treated separately to calculate overlap properties.
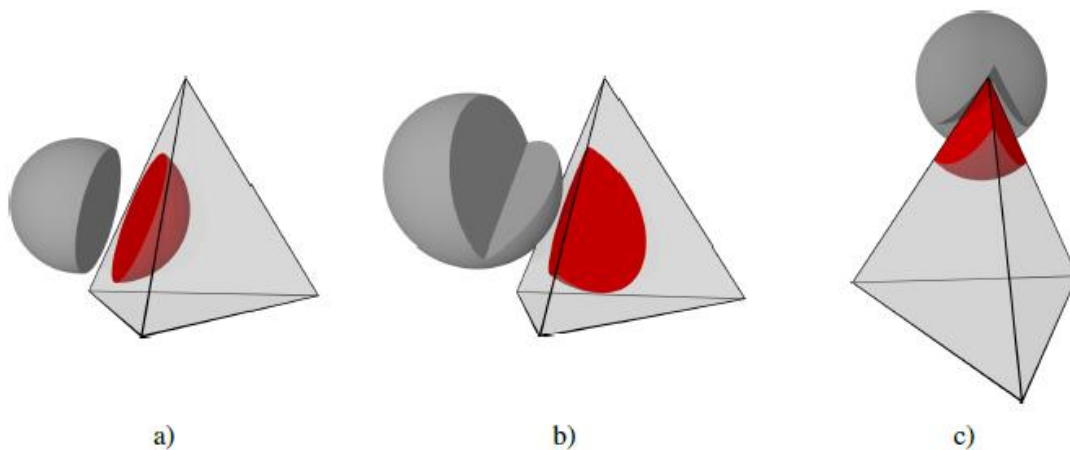
Figure 24: Possible Overlap Geometries a) Face Overlap; b) Edge Overlap; c) Vertex Overlap [21]

Vertex Overlap

Sphere is in contact with a vertex if the distance between centre of sphere and vertex is less than radius of the sphere. If vertex A is overlapping with sphere

$$d < r \ \text{ where } d = |A|$$

Edge Overlap

To check the overlapping of edge AB and sphere, first overlapping of line containing edge AB and sphere has to be checked. For overlapping of line and sphere

$$d < r \text{ where } d = |Q|$$

However since line is infinite length, the overlap points can be outside of AB of the tringle. Therefore overlapping points has to be calculated and checked whether they are within AB. This check has to be done after vertex overlap check because; overlapping condition for edge overlap is true in vertex overlap by default. Since edge overlap comes after vertex overlap, checking of one intersection point is sufficient.
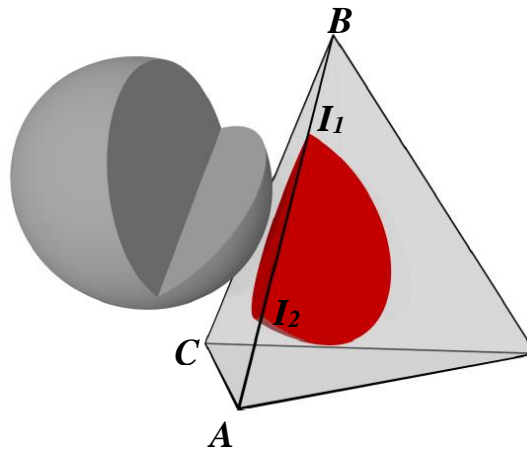
Figure 25: Intersection points for edge overlap

To calculate intersection point; substitute equation of line in equation of sphere and transform to quadratic equation form [20].

$$at^2 + bt + c = 0 \tag{21}$$

Where;

$$a = |B - A|^2$$

$$b = 2[(x_B - x_A)x_A + (y_B - y_A)y_A + (z_B - z_A)z_A]$$

$$c = |A|^2 - r^2$$

The solution for quadratic equation is;

$$t = \frac{-b \pm \sqrt{b^2 - 4ac}}{2a} \tag{22}$$

Notice that 't' has two solutions giving two intersection points. Intersection point can be calculated;

$$I = A + (B - A)t \tag{23}$$

Then point I has to be checked to be inside AB. If I is between AB angle between IB and IA vectors has to be 180°. Therefore;

$$(A - I).(B - I) < 0$$

If both conditions are satisfying then sphere is overlapping with edge AB.

Face Overlap

Face overlap is the last condition of the developed algorithm. If triangle has no separation axes, neither vertex nor edge overlap, the only possible solution has to be face overlap.

7.3   Ice-Structure overlap properties calculation

After identifying the overlaps, overlap properties has to be calculated. As the first step geometry of the overlap part has to be defined. Until this step structure is represented by surface mesh. However to calculate the overlap properties, a 3D mesh is required. Triangular surface mesh of the structure element can be converted to a solid tetrahedron mesh by joining all the triangle vertices to the centre of gravity of the structure. Since structure elements are convex, these lines are not crossing each other. Therefore when a sphere is overlapping with a triangle on surface, overlap geometry is obtained from overlapping a sphere and a tetrahedron. Then geometry of overlap volume can have three possibilities according to the overlap cases from contact detecting algorithm. General shape of the overlap volume is illustrated in figure 24. Above three cases have to be handled separately.

7.3.1 Face Overlap

Overlap geometry formed in face overlap case is a spherical cap. Volumetric properties of spherical cap can be calculated as following.
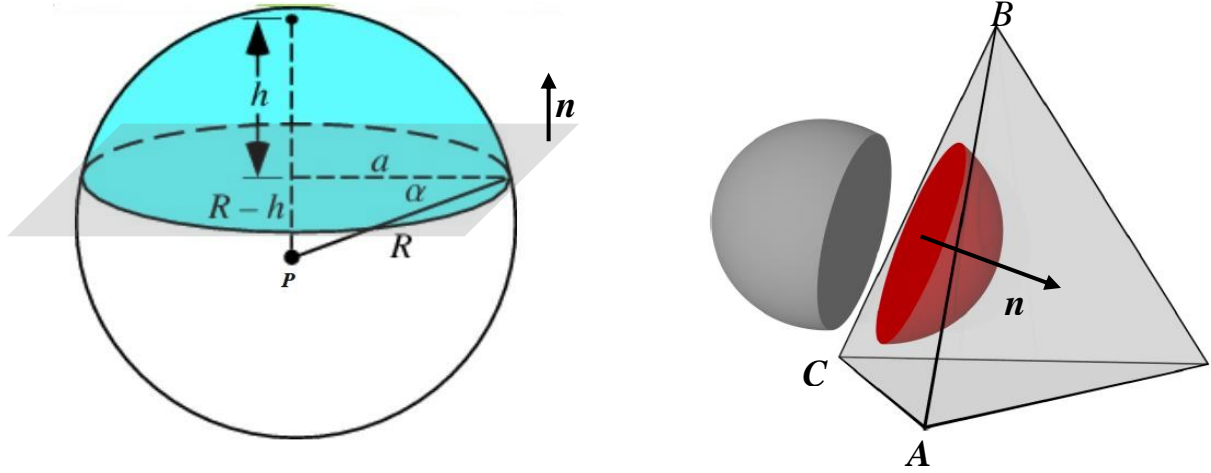
Figure 26: Volume of spherical cap

Normal direction of triangle plane and unit normal vector;

$$V = (B - A) \times (C - A)$$

$$n = \frac{V}{|V|}$$

$$d = n.(P - A)$$

$$h = r - d$$

$$Overlap\ Volume = \frac{\pi h^2}{3}(3r - h)$$

To calculate centroid and force direction a different approach is needed. In this case force direction is normal to plane of the triangle face.

However in this case direction of the normal vector has to be checked with respect to centre of sphere. Therefore;

$$n.(P - A) > 0$$

Overlap centre of gravity with respect to sphere centre can be calculated as follows.

$$CG = \frac{3(2r - h)^2}{4(3r - h)}$$

To find overlap centre of gravity in global coordinates;

$$Overlap\ Centroid = P + (-n).CG$$

$$center\ of\ spher = P$$

Here n is negative since force direction is defined towards the sphere and centre of gravity is located away from centre.

7.3.2 Edge Overlap

Overlap geometry in edge overlap has shape of general spherical wedge. However there are no closed analytical expressions to calculate the volumetric properties of a general spherical wedge. Therefore this geometry is decomposed in to two sub geometries having shape of regularized wedge. Regularized wedge is spherical wedge with one of its two intersection plane passes through the centre of sphere. Regularized wedge has exact analytical solution for volumetric properties.
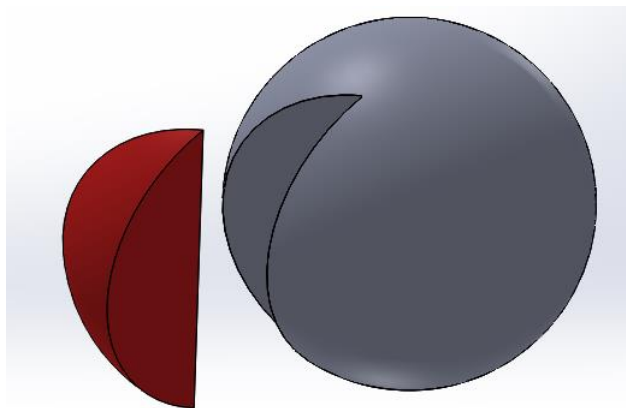
Figure 27: Edge overlap geometry

Volume of General Spherical Wedge

Spherical wedge is the cut out volume of a sphere by two intersecting planes. Planes can intersect anywhere inside the sphere and angle between planes can be also arbitrary. Take two planes p_0 and p_1 defined by points A, B, C and A, B, CG. Here A, B, C are the vertices of the face triangle, CG is the centre of gravity of the structure element and AB is the common overlapping edge of tetrahedron. For all cases of p_0 and p_1, a third plane p_s can be created, such that p_s is perpendicular to p_0, p_1 and going through sphere centre. Decomposition of general wedge in to two regularized wedges can be described using the projection of sphere

and p_0, p_1 onto p_s. Based on the relative position of p_0 and p_1 with respect to the centre of sphere, three different decomposition cases can be found. These cases has to be identified and treated separately to calculate volumetric properties.
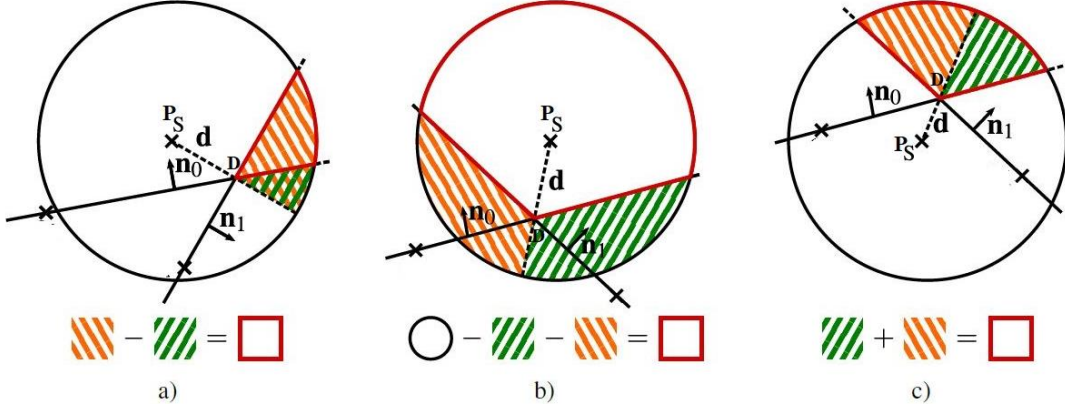
Figure 28: Decomposition of general wedge-red outline is the required volume [21]

General Wedge Calculation Procedure

As the first step normal vectors to plane ABC and ABCG (n_0, n_1) have to be calculated from equation 18. In this case the normal vector should be going into the direction of tetrahedron. Then separation vector from sphere centre to p_s has to be calculated. The separation point is the midpoint between two intersection points of sphere and edge AB using equations 21 to 23. Then separation point D, separation vector d_sep and unit vector in the direction of d;

$$D = \frac{I_1 + I_2}{2} \qquad d\_sep = D - P \qquad d = \frac{d\_sep}{|d\_sep|}$$

Then cosine of angle between two regularized wedges can be calculated;

$$s_0 = d.n_0 \qquad s_1 = d.n_1$$

The three cases of general wedges are dependent on sign of s_0 and s_1. For small angles of regularized wedge, cosine value are positive and for angles large than 90, cosine values are negative. However first a special case of s_0 or s_1 equals zero has to be handled. In this case one of the planes of p_0 or p_1 passing through the centre and overlap volume is originally a regularized wedge. Since it is unable to achieve the exact zero in computer numerical simulations, a limiting value ε (10e-10) is used. Therefore

$$If \ s_0 < ε \ or \ s_1 < ε \quad calculate\_regularized\_wedge(rad, |d\_sep|, α, \min(s_0, s_1))$$

In this case *calculate_regularized_wedge* is a function to calculate volumetric properties of regularized wedge, where inputs are radius of sphere, magnitude of separation vector, angle

between planes of regularized wedge and cosine of angle between two regularized wedges. Outputs are overlap volume, overlap area and overlap centre of gravity with respect to centre of sphere. Definition and computations within this function are explained in the next section.

In this special case;

$$\alpha = \pi - angle(n_0, n_1)$$

Having s_0 and s_1 are sufficiently large enough, analysis for the three main cases can be done. First angles of regularized wedge has to be calculated to get the correct configuration. Projection of plane on d can be used to determine the correct configuration as shown in the figure 27.

$$d_0 = [C - (I - p)].d$$
$$d_1 = [CG - (I - p)].d$$

(24)

In the second expression CG refers to the point CG of A, B, CG plane and not the CG of overlap volume. I is the intersection point of edge AB and sphere which is calculated using equation 23 (figure 26).

Case C: $s_0 \geq 0 \ and \ s_1 \geq 0$

In this case overlap volume composed of regularized wedges with centre of sphere is outside the overlap volume. Respective angles of regularized wedges can be calculated.

$$\alpha_0 = \frac{\pi}{2} - angle(n_0, d).sign(d_0)$$
$$\alpha_1 = \frac{\pi}{2} - angle(n_1, d).sign(d_1)$$

(25)

Then;

$$calculate\_regularized\_wedge\_1(rad, |d_{sep}|, \alpha_0, s_0)$$

$$calculate\_regularized\_wedge\_2(rad, |d_{sep}|, \alpha_1, s_1)$$

$$Overlap\ Volume = V\_reg_1 + V\_reg_2$$

$$CG = \frac{V\_reg_1 CG\_reg_1 + V\_reg_2 CG\_reg_2}{V\_reg_1 + V\_reg_2}$$

(26)

Since the CG is given with respect to center of sphere,

$$Overlap\ Center\ of\ Gravity = P + CG.d$$

In this case only one overlap surface is outside the structure and the other is inside. Therefore overlap area has to be from outer triangle only. In addition force is applied only on this surface. Therefore force direction should be the normal direction of plane containing outer triangle and it should be to the outside direction with respect to overlap volume.

$$Overlap\ Area = A\_reg_1$$

$$Force\ Direction = -n_0$$

Case B; $s_0 < 0\ and\ s_1 < 0$

In case B, general wedge is composed of two regularized wedges with centre of sphere is inside the overlap volume. Therefore overlap volume has to be computed by subtracting the volumes of regularized wedges from volume of the sphere. The angle of regularized wedges can be calculated as;

$$\alpha_0 = \frac{\pi}{2} + [angle(n_0, d) - \pi].sign(d_0)$$

$$\alpha_1 = \frac{\pi}{2} + [angle(n_1, d) - \pi].sign(d_1)$$

(27)

Then;

$$calculate\_regularized\_wedge\_1(rad, |d_{sep}|, \alpha_0, -s_0)$$

$$calculate\_regularized\_wedge\_2(rad, |d_{sep}|, \alpha_1, -s_1)$$

$$Overlap\ Volume = V_{sphere} - (V\_reg_1 + V_{reg_2})$$

$$CG = \frac{V\_reg_1 CG\_reg_1 + V\_reg_2 CG\_reg_2}{V_{sphere} - (V\_reg_1 + V_{reg_2})}$$

(28)

Then overlap centre of gravity on global coordinates can be found same as equation 26. Overlap area and force direction are also same as the case C; overlap area with regularized wedge 1 and force direction normal to outer triangle face.

Case A; s_0 and s_1 have opposite signs

In this case general wedge is formed by subtraction of two regularized wedges. Centre of sphere can be located anywhere with respect to overlap volume. Regularized wedge angles can be calculated;

$$\alpha_0 = \frac{\pi}{2} - [angle(n_0, d) - (if\ s0 < 0\ then\ \pi\ else\ 0)].sign(d_0 \times s_0)$$

$$\alpha_1 = \frac{\pi}{2} - [angle(n_1, d) - (if\ s1 < 0\ then\ \pi\ else\ 0)].sign(d_1 \times s_1)$$

(29)

Then;

$calculate\_regularized\_wedge\_1(rad, |d_{sep}|, \alpha_0, |s_0|)$

$calculate\_regularized\_wedge\_2(rad, |d_{sep}|, \alpha_1, |s_1|)$

$$Overlap\ Volume = \max(V\_reg_1, V\_reg_2) - \min(V\_reg_1, V\_reg_2)$$

Centre of gravity can be calculated from equation 26 accordingly. Overlap area and force direction are from regularized wedge 1 in this case as well.

Regularized Wedge Calculation

As explained earlier, regularized wedge is a special case of spherical wedge where one of two constructing planes is passing through the centre of the sphere.
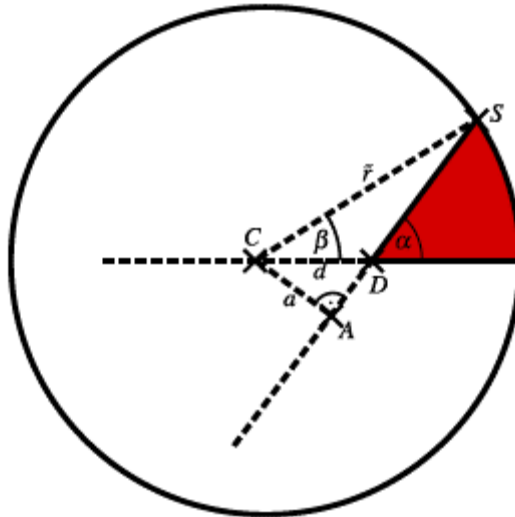
Figure 29: Regularized wedge on projected plane [21]

Volume of regularized wedge can be calculated by;

$$V = \frac{1}{3}abc + a\left(\frac{1}{3}a^2 - r^2\right) + \frac{2}{3}r^3 \arctan\left(\frac{b\sin\alpha}{r\cos\alpha}\right) \tag{30}$$

With $a = d\sin\alpha \qquad b = \sqrt{|r^2 - d^2|} \qquad c = d\cos\alpha$

There is no exact analytical formulas to calculate the centre of gravity of regularized wedge. Therefore to ease the calculations, it was assumed that centre of gravity of regularized wedge is on area centre of the arc segment on projected plane.

7.3.3 Vertex Overlap

In vertex overlap, overlap geometry has a shape of a tetrahedron with one spherical cap face. There are no exact analytical formulas to calculate overlap properties in this case as well. Therefore the overlap volume is divided into several known geometrical bodies: a tetrahedron and a spherical cap with three general wedges removed from sides. Using the same notation from above section and vertex A being the overlapped vertex;
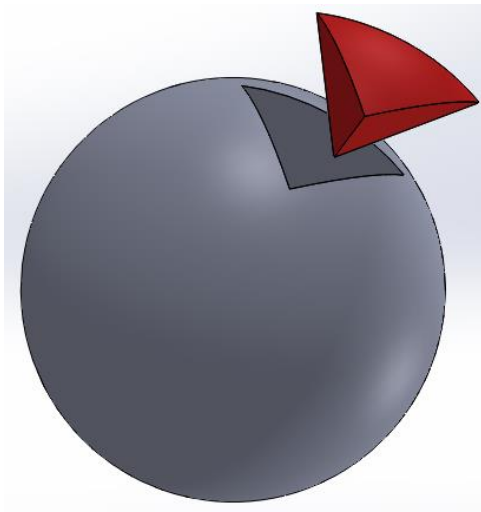
Figure 31: Vertex overlap geometry   *Figure 30: Decomposition of overlap volume*
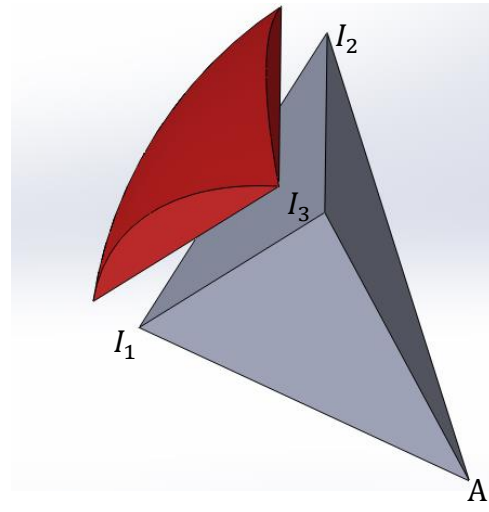
$$Overlap\ Volume = V_{tet} + [V_{cap} - (V_{wedge1} + V_{wedge2} + V_{wedge3})] \tag{31}$$

To calculate the volume of tetrahedron, intersection points of sphere and AB, AC, ACG edges are needed. Equations 21 to 23 can be used and same procedure is followed. If intersection points are I_1, I_2, I_3 volume of tetrahedron is;

$$V_{tet} = \frac{1}{6}|(I_3 - A).[(I_2 - A) \times (I_3 - A)]| \tag{32}$$

$$CG_{tet} = \frac{1}{4}[A + I_1 + I_2 + I_3]$$

Calculating the volumetric properties of spherical cap is similar to face overlap case. In this case three general wedges have to be subtracted from spherical cap. The wedges will be formed by intersecting faces of structure element tetrahedron and plane I_1, I_2, I_3. Three wedges can be calculated using the general wedge calculating procedure. Having calculated all the volumes, overlap volume can be calculated from equation 31. To calculate centre of gravity;

$$CG$$
$$= \frac{V_{tet}.CG_{tet} + [V_{cap}.CG_{cap} - (V_{wedge1}.CG_{wedge1} + V_{wedge2}.CG_{wedge2} + V_{wedge3}.CG_{wedge3})]}{V_{tet} + [V_{cap} - (V_{wedge1} + V_{wedge2} + V_{wedge3})]}$$

In this as well, force direction is in the normal direction to triangle ABC, All the other faces are inside the structure tetrahedron element. Equation 18 can be used to calculate the normal force direction and has to be checked for the correct direction.

Above procedure explains the overlap detection and overlap properties calculation between sphere and a single triangle. However in the simulation structure is made of triangular mesh. Therefore a spherical ice particle will be in contact with multiple triangular mesh elements. Hence a cumulative loop was introduced in the Ice-Structure contact detection algorithm to compute overlap properties. Loop is running the overlap detection check for all the triangle mesh elements of the structure. Once an overlap of ice particle and triangle is identified, corresponding overlap properties are calculated. Then loop is continued to again. Equations for cumulative addition is;

$$V_{overlap} = V_{overlap} + V_{overlap\_new}$$

$$CG_{overlap} = \frac{V_{overlap}.CG_{overlap} + V_{overlap\_new}.CG_{overlap\_new}}{V_{overlap} + V_{overlap\_new}}$$

$$Force\ Direction = \frac{A_{overlap}.Force\_Direction + A_{overlap_{new}}.Force\_Direction_{new}}{A_{overlap} + A_{overlap\_new}}$$

Since only the direction is required, force direction has to be converted in to a unit vector.

Since the overlap test is done on all the mesh triangles of a structure element, having larger structural elements with high number of triangles faces can slow down the simulation. For large elements, there can be many possible overlap cases from axis aligned bounding box sorting.

Then triangle-sphere contact detection has to be performed on all these possible cases to identify actual overlaps. This can be avoided by having adequate number of smaller structure elements. Then bounding box sorting will be more refined and number of possible overlaps would be less. In addition, subdividing structure so that waterline is in between a small structure elements, will also decrease the possible overlap cases from axis aligned bounding box sorting and speed up the simulation. This is further explained in section 12.2 ship model preparation.

8 Calculating Forces

To apply dynamic equation on DEM, all the forces acting on elements have to be calculated. Different types of forces are acting on elements according to their relative position and interaction between other elements. A summary of considered forces is given in following table.

Table 2: Summary of forces acting on ship and ice

Force	Applied Elements	Force Direction	Generates Moment	Calculation Method
Elastic	Ice/Ship	Normal to interface of contact area	Yes	Hertzian contact law: elastic forces are proportional to the overlap volume
Normal Damping	Ice/Ship	Normal to interface of contact area	Yes	Damping forces are proportional to the rate of change of overlap volume
Friction	Ice/Ship	Tangential to interface of contact area	Yes	Cundall-Strack Friction model: friction forces calculated by incrementing force in previous time step
Dissipation	Ice/Ship	Tangential to interface of contact area	Yes	Dissipative tangential fore due to collision of elements: depend on velocity of contact
Cohesion	Ice	Normal to interface of contact area	Yes	Cohesion force due to overlap of ice rubbles: depend on contact area

Viscous Drag	Ice	Tangential to the velocity vector	Yes	Hydrodynamic viscous drag on ice rubbles: calculated by classical drag coefficient method
Buoyancy	Ice/Ship	Vertically downward	Yes	Ice rubbles: Buoyancy force of ice rubbles calculated by displaced volume by element Ship: ship hydrostatic are obtained from pre calculated data array
Gravity	Ice/Ship	Vertically Upward	Yes	Ice rubbles: Gravity force is calculated from density and volume of element Ship: ship weight is taken equal to buoyancy force in the initiation since it is floating, then it is kept constant
Propeller Thrust	Ship	Horizontal to the direction of ship movement	No	Propeller thrust on ship is calculated from propeller open water characteristics. Classical thrust coefficient method is used.
Open water Resistance	Ship	Horizontal to the opposite direction of ship movement	No	Only the viscous drag of open water resistance is considered. Calculated from drag coefficient in input.

Above force can be divided in to two groups according to the force definitions. They are contact forces and external forces. Contact forces are generated due to collision of two elements. External forces such as gravity, buoyancy and drag are independent forces acting on elements and can be calculated from their usual definitions.

8.1 Contact Forces

Contact force model in DEM can be given in figure 31. Contact forces are on both normal and tangential directions to the collisions. Normal direction is defined by the perpendicular to the contact surface. This is calculated in the overlap geometry computational step. Then tangential direction can be defined perpendicular to normal direction. All contact forces are to be assumed to act from centre of gravity of overlap volume which is also calculated in overlap computation step.
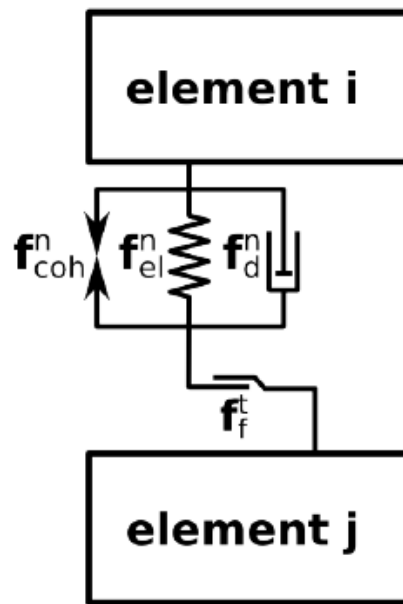
Figure 32: DEM contact force model

8.1.1 Elastic Force

Elastic Force is the normal reaction force of collision between two particles. Elastic normal force can be modelled by Hooks law and force is proportional to deformation. For rigid particles in DEM, deformation can be replaced by overlap between two particles, and this will lead the contact force to Hertz model. In this case spring constant for Hook's law will not be same as the Young's modules of material and will act as an internal parameter of simulation. Optimum value for Young's modules has to be found by sensitivity analysis.

$$F_{el} \propto Y \times V_{overlap}$$

When considering the units of elastic force law with Young's modules and overlap volume, resulting units are not those of force. The length dimensions are not cancelled out. Therefore additional length dimension parameter has to be in the equation. This can be derived based on

the sound velocity for space filling packing of particles. Sound velocity in space filling packings in DEM simulation should be independent of particles sized and has to be same as the sound velocity of bulk material. Therefore product of overlap volume and Young's modules has to be divided by a length factor called characteristics length.

$$l_c = 4 \frac{|r_1| \cdot |r_2|}{|r_1| + |r_2|}$$

Where r_1 and r_2 are the position vector of centre of gravity of the two colliding elements.

Then force equation can be given as;

$$F_{el} = \frac{Y \times V_{overlap}}{l_c}$$

8.1.2 Damping Force

When two particles collide with each other, there is an energy dissipation. Part of this energy dissipation can be modelled as a normal damping force between particles. The other part is accounted for frictional forces in tangential direction. Normal damping force can be calculated from;

$$F_d = \gamma^n \sqrt{\frac{Y M_{red}}{l_c^3}} \frac{\delta V_{overlap}}{\delta t}$$

Where γ^n is normal damping coefficient, M_{red} is reduced mass of overlapping elements and $\delta V_{overlap}/\delta t$ is rate of change of overlapping volume. In this case reduced mass is a parameter introduced to compensate the effect of size difference of two overlapping particles. Reduced mass is calculated from mass of two overlapping elements m_1 and m_2. For wall elements which are not moving, very high hypothetical mass values are introduced in the simulation, so that overall reduced mass is equal to mass of the particle.

$$M_{red} = \frac{m_1 m_2}{m_1 + m_2}$$

Rate of change of overlap volume is calculated numerically using, overlap volume of previous step and time step.

$$\frac{\delta V_{overlap}}{\delta t} = \frac{V_{overlap}(step\_n) - V_{overlap}(step\_n - 1)}{dt}$$

When two elements are separating after a collision, rate of change of volume is becoming negative, adding a pulling force against separation. However for faster separations, this pulling force might become larger than elastic reaction, causing an unrealistic attraction. Therefore a cut off limit has to be implemented.

$$if\ F_{el} + F_d < 0\ then\ F_d = -F_el$$

8.1.3 Friction Force

There is a friction force between two sliding elements, in the tangential direction. Generally this friction force can be model using Coulomb Friction Theory. However it is complicated to numerically implement the Coulomb Friction model. Therefore Cundall-Strack model is implemented in the simulation. In this method sliding friction at particular time step, is incremented from previous time step given that there is sliding. Amount of increment is proportional to the tangential contact velocity and tangential stiffness which is stiffness of material in the tangential direction. An upper limit for friction force has to be implemented since tangential friction cannot exceed the sliding Coulomb friction. Different frictional behaviour of ice-ice contacts and ice-structure can be observed in experiments. Hence for ice-ice contacts high friction coefficient is used and for ice-structure contacts low friction coefficient is used. Cundall-Strack model is defined neglecting the cohesion between particles. Therefore calculating of friction has to be done before the addition of cohesion forces to the normal forces in the simulation.

Calculation of Cundall-Strack Friction Force

As the first step friction force from previous time step is projected to new tangential plane. Tangential plane changes in each time step due to change of normal direction.

$$F_f^p(t - dt) = F_f(t - dt) - [F_f(t - dt).n(t)]n(t)$$

Here p is for new tangential plane and n is the unit vector in normal direction.

Next magnitude of the projected friction force has to be scaled to the previous value.

$$F_f^r(t - dt) = |F_f(t - dt)|.\frac{F_f^p(t - dt)}{|F_f^p(t - dt)|}$$

Increment of friction force based on tangential stiffness model.

$$F_f(t) = F_f^r(t - dt) - k_t v_t(t) dt$$

Tangential stiffness in the simulation is calculated based on the Poisson Ratio.

$$k_t = vY$$

Finally a cut off is implemented to avoid friction force exceeding the sliding friction.

$$if \ |F_f| > \mu|F_n| \ then \ F_F = \frac{F_f}{|F_f|} . \mu|F_n|$$

Here F_n is the normal reaction force

$$F_n = (F_{el} + F_d). n_0$$

8.1.4   Cohesion Force

Ice particles have bonding action when collided, which can be model by a cohesion force. Cohesion force can be calculated as;

$$F_{coh} = k_{coh} Y A_0$$

k_{coh} is the cohesion coefficient for ice and it is a fraction of Young's modules. A_0 is the contact area which is calculated in overlap geometry calculation section. As explained earlier cohesion force has to be added to normal force after calculation of friction.

Therefore total normal force at this step is;

$$F_n = F_n - F_{coh}. n_0$$

Theoretically a damping force in the tangential direction has to be added as well. However tangential damping caused the simulation to be unstable. Magnitude of tangential damping is low, so it was neglected. Hence the only tangential force is friction force. Total vector of contact forces can be calculated as;

$$F_{contact} = F_n + F_f$$

This contact force will be acting on both of the elements in contact as action and reaction. Since the force is acting on centre of gravity of the overlap volume, there is resultant contact torque on elements as well.

$$T_{contact} = (CG_{overlap} - CG_{element}) \times F_{contact}$$

This torque has to be calculated separately for two overlapping elements, since lever arm for torque dependent on the size of the particles.

8.2 External Forces

8.2.1 Drag Force

Ice particles in water subjected to drag force when in motion. This can be viscous drag and pressure drag. In the numerical tool it is complex to implement pressure drag, therefore only the viscous drag is considered. Since particles are moving in slow speeds, dominance of pressure drag is much less compared to viscous drag. Viscous drag on spherical particle can be calculated by;

$$F_{drag} = -\frac{1}{2} C_d \rho A |v|^2 . \frac{v}{|v|}$$

Drag force is to the opposite direction of particle movement. C_d is the drag coefficient for a sphere which is 0.47. A is the cross sectional area of the particle which is calculated in the ice elements initiation. Since some particles are on free surface, cross section area is dependent on the position of the particle. Therefore a check was implemented to detect the position of ice particles and calculate cross section areas accordingly.

In the case of cylinder experiment, drag on the cylinder has to be considered. Same equation was used to obtain viscous drag on cylinder with C_d 0.82 with respective cross section area. Wave making resistance on cylinder is neglected due to slow speed.

In case of ship model experiment, it is not possible to calculate the hydrodynamic drag on ship with simple calculations. In addition there are many commercial codes available to estimate the open water resistance. Therefore open water resistance at design speed was taken as an internal parameter of the code. User has to input the open water resistance of the model at design speed and resistance for other speeds are estimated by code using the drag equation assuming drag coefficient and wetted area does not change significantly with the speed.

8.2.2 Buoyancy Forces

Ice particles submerged in water are subjected to a buoyancy force. Buoyancy force on ice particle can be calculated by;

$$F_b = -V\rho g$$

Here V is the submerged volume of the ice particle and it is calculated in particle initialization. Buoyancy force has negative sign since the positive Z direction of the simulation domain is towards the tank bottom. As similar to drag force, submerge volume of the particle changes as it comes to free surface. Therefore a check was implemented to detect the position of ice particles and calculate submerged volume accordingly.

In case of cylinder experiment, buoyancy force on cylinder can be calculated using the same equation with respective submerged volume. However in case of ship, it is too computationally expensive to calculate the buoyancy force on ship each step because of the complex shape. Therefore as explained in the DEM algorithm for ship simulation, a hydrostatic data table is calculated in the initiation. Draft, pitch ad roll of the ship is varied within given range and buoyancy force and centre of buoyance is calculated for each case. This data is stored in a data array. When simulation need the buoyancy forces in min calculation loop, program refers to buoyancy data array and estimate the buoyancy force and centre o buoyancy by tri-linear interpolation of draft, pitch and roll [14].

8.2.3 Gravity Forces

All the elements in the simulation are subjected to gravity force. For ice particles, gravity force can be calculated by;

$$F_g = V\rho_{ice} g$$

For structures, total mass has to be given as an input by the user. In case of ship in addition to the mass at the design draft, centre of gravity has to be input as well. For ship simulations, this data should match with buoyancy calculation by the code, to stabilize the vessel properly in simulation. Any mismatch can cause ship to go unstable giving unrealistic results.

8.2.4 Propeller Thrust

Propeller thrust has to be calculated for the ship self-propulsion test. Performance characteristics of a propeller is usually given by propeller open water tests. Same approach is used in the code, where user has to input the propeller characteristics as a test file and code will be calculating propeller thrust accordingly. These propeller characteristics are obtain by an open water test in a cavitation tunnel. Since the interest of simulation is on self-propulsion point, user has to input propeller characteristics at the desired RPM. Input contains propeller RPS, diameter, number of propellers, wake fraction, thrust deduction factor and table of advance ratio vs. thrust coefficient. Although thrust deduction factor is not propeller parameter, it is needed for correct thrust calculation, hence included with propeller. At a particular ship speed, advance ratio can be calculated as;

$$J = \frac{V_a}{N.D}$$

Here N is the RPS and D is the propeller diameter. V_a is advance velocity of the propeller in the ship flow. Since propeller is operating in the wake created by ship hull, advancing velocity of propeller is lower than ship velocity which can be calculated as follows.

$$V_a = (1 - w)V_s$$

In the equation w is wake fraction and V_s is ship speed and w is wake fraction.

Then relevant thrust coefficient corresponding to the advance ratio can be found from the table using liner interpolation. Next propeller thrust can be calculated using following formula.

$$T = K_T \rho N^2 D^4$$

Since the equations are for one propeller, total thrust developed by propeller can be obtain from multiplying the thrust value by number of propellers.

$$T_{prop} = T.n_{prop}$$

Since the ship open water resistance is obtained from towing tank or open water simulation test, influence of propeller pressure filed in hull has not been taken in to account yet. Therefore finally this augmented of resistance is corrected using thrust deduction coefficient.

$$T_{result} = (1 - t)T_{prop}$$

Here 't' is he thrust deduction factor.

9 Corrector Step: Equation of Dynamics

Having calculated all the forces, equations of motion can be applied for elements, with calculated forces. Newton's second law is used for transition moments in ordinary form. For rotational movements, Euler's rotational equations are used with Quaternions to assure the numerical stability of the scheme. For an ice particle, resultant forces can be calculated as;

$$F(t) = F_b + F_g + F_d + \sum_{j=1}^{l} F_{contact}(t)$$

Next transitional acceleration can be obtained from;

$$F(t) = m\ddot{x}$$

Where; $F = force, m = mass \ and \ \ddot{x} = acceleration$

For rotational movements,

$$\tau = I\omega$$

Here w is angular velocity and I is inertia tensor with respect to fixed coordinate system. However, in practise it is difficult to compute inertia tensor for a moving particle with respect to space fixed coordinate system. Therefore a rotation matrix is used to transform inertia tensor of particle from a body fixed coordinate system to space fixed coordinate;

$$I^s = RI^b R^T$$

Where S denotes space fixed coordinate system, b denotes body fixed coordinate system and R is the rotation matrix in standard form. However using rotation matrix can lead to singularities when transforming angles and components of rotation matrix. Therefore, it is suggested to use quaternions. Quaternion is a complex number representation of position vector of a particle.

$$q = w + xI + yJ + zK$$

w is the scalar representation of vector while I, J and K are complex numbers. To write the equation of moment it requires angular velocity and its rate of change. Therefore, relationship between angular velocity and quaternions can be expressed as;

$$\dot{q} = \frac{1}{2}\omega q \qquad and \qquad \ddot{q} = \frac{1}{2}(\dot{\omega}q + \omega\dot{q})$$

With above equations, moment equation can be derived, and solved numerically by Gear's predictor algorithm. From Gear's correction method;

$$r_c^{t+\delta t} = r_p^{t+\delta t} + c_0. \Delta \ddot{r}$$

$$\dot{r}_c^{t+\delta t} = \dot{r}_p^{t+\delta t} + c_1. \Delta \ddot{r}$$

$$\Delta \ddot{r} = \ddot{r}^{t+\delta t} - \ddot{r}^t$$

$$\ddot{r}^{t+\delta t} = \frac{F^t}{m}$$

Here subscript c denotes the corrected value, $c_0 = 0$, $c_1 = 0.5dt$

For quaternions;

$$q_c^{t+\delta t} = q_p^{t+\delta t} + c_0. \Delta \ddot{q}$$

$$\dot{q}_c^{t+\delta t} = \dot{q}_p^{t+\delta t} + c_1. \Delta \ddot{q}$$

$$\ddot{q}_c^{t+\delta t} = \ddot{q}_p^{t+\delta t} + c_2. \Delta \ddot{q}$$

$$\Delta \ddot{q} = \ddot{q}^{t+\delta t} - \ddot{q}^t$$

$$\ddot{q}^{t+\delta t} = \frac{1}{2}(\dot{\omega}^t q^t + \omega^t \dot{q}^t)$$

Where $c_0 = 0$, $c_1 = 0.5dt$, $c_2 = 1$

10 Program Output

Simulation results are written in several output files, according to the simulation option. Mainly results can be divided in to two categories; numerical results and graphical results. Numerical results are in .csv file format which can be open through spreadsheet software. Graphical output is in .vrk format, which has to be open by a visualization software such as ParaView.

10.1 Numerical Outputs

In all three options of the simulations, total kinetic energy of the system is recorded at each time step. Purpose of this is to monitor the simulation. Time evolution of kinetic energy in the system has to be smooth in normal conditions. In case of Channel Generation, final numerical results are in .txt format. These results include, definitions (radius, mass, inertia), final positions, final velocities, overlapping elements list and neighbouring elements list for all ice particles in channel. These files are used to recreate the channel again in case of cylinder experiment and ship model test. Therefore once a channel is generated, it can be used for many simulations, saving time and effort.

In cylinder experiment, data logging .csv files are created for cylinder position, advancing velocity, acceleration and forces along three axes. Results are written in to file at each time step for monitoring purposes. However since simulation can last up to several million time steps, it is not possible to analyse these results using a normal spread sheet software. Therefore for post processing purposes, these files have to be imported to DIAdem. DIAdem is a software package used for analysis of electronic measurements from sensors. Therefore it can easily handle the large amount of data and can be used to post process and visualize data. Since it is time consuming to analysis all the data in monitoring stage, an additional result file with critical data such as forces and velocity is generated. However the interval for writing data to this file is much higher, about few thousands of time steps. The time interval for data logging in this file is similar to graphical output file generation interval which will be discussed later in this chapter. A quick real-time overview of simulation can be obtained checking this file during the simulation. In case of ship model test, a similar file structure was followed. Output files are generated same as cylinder experiment and have to be handled similarly.

10.2 Graphical Output

For all three options graphical output files are create in .vtk legacy serial format. In .vtk file it contains information about all the points which produce the object and how they are formatted. Since simulation time step is very small, generating graphical outputs for every step is not very practical. In-fact a human eye can't detect, changes of screen faster than 25 frames per second. Therefore having time interval smaller than this, between two graphical output files is useless. However there can be some requirements to view the ship motions in slow motion. Therefore 40 FPS frame rate was used in the simulation. Then number of time steps between two graphics output files can be calculated from following equation. As explained earlier, interval for overall results file was also kept the same, so that numerical values can be compared with graphical output.

$$w_{interval} = int(\frac{1}{dt.fps})$$

As explained in the earlier chapters, simulation contains two types of elements. Structures are defined with triangulated surface mesh elements and ice particles are spherical elements. Generally in .vtk files, objects are defined using polygonal definitions. File contains a list of all the vertices forming polygonal and then a list of which vertices forms which vertices. This is very efficient in representing structure elements, since they are already stared in the arrays of simulation in this format. However in case of ice particles, spheres just has definition of centre and radius with a continuous surface. In computer graphical representation, it is not possible to represent continuous surface and, usual practice is to mesh the surface triangles for graphical representations. ParaView has an internal function to generate spherical Glyph objects given the centre and radius. However this requires an unstructured grid data format in .vtk files. Therefore two different graphical output files are created for ice and structure in each graphics output step. These two file types can be loaded together in ParaView for visualization.

In addition to the objects, .vtk file can also represent some data relevant to the elements such as velocity. Therefore element velocity is also included as a point data in .vtk file. In ParaView particle velocity can be represented by a colour scheme, for visualization. This is very helpful in determining force paths in ice and to analyse far field behaviour.

Part III: Cylinder Experiment and Sensitivity Analysis

11 Cylinder Experiment

Cylinder Experiment is a reference test used in ice tanks to compare brash ice channel properties. The test is carried out after preparing of each ice channel. HSVA has reference data for these tests and properties of channels can be compared with these results. In brash ice DEM simulation tool, cylinder experiment was implemented for the same reason. Tool can be calibrated by a sensitivity analysis based on the cylinder experiment.

Figure 33: Cylinder experiment in ice tank

11.1 Sensitivity Analysis

Sensitivity analysis is a test to determine the influence of simulation parameters on results. In the test, simulation parameters are changed in a suitable range and change of the results are studied. There are many internal parameters in the developed tool, which influences the results. However four parameters were identified as crucial and, sensitivity analysis was limited to those four parameters. Parameters were selected based on the literature and, previous work on DEM simulation of ridge breaking [17]. Simulations were based on a specific cylinder experiment carried out in the tank. Therefore all the results are compared with the experimental results in the end of the section. Following parameters are used in all the simulations.

Table 3: Channel properties

Channel length	10 m
Channel width	2 m
Brash ice thickness	45 mm
Porosity	0.35
Cylinder diameter	200 mm
Towing speed	0.74 m/s
Bending strength of ice	5×10^4 N/m^2

11.1.1 Influence of Time Step

As explained in the predictor and corrector steps, a fixed time step is used for numerical integration of equations of motion. Optimum time step is important for correct results and performance of DEM simulations. Having bigger time step might cause excessive overlap volumes, unstable simulations and distorted results. Nevertheless a smaller time step means, higher number of steps to complete the simulation. Therefore time step has to be optimum to obtain acceptable results in efficient way. Time step can be calculated by given formula.

$$dt = 2frac\sqrt{\frac{m_{min}}{2Y_{max}}}$$

Where, m_{min} is the minimum mass of a particle, Y_{max} is the largest normal or shear contact stiffness and frac is a user defined factor. In the code, m_{min} is obtained by searching mass of all the particles in the simulation. For ice-structure simulations with relatively large structure elements and small ice particles, contact stiffness is breaking strength of ice. Parameter frac was changed in the sensitivity analysis to obtain an optimum value. For ridge ice simulations, optimum frac value was chosen as 0.1. Since ice particles of brash ice are much smaller than ridge ice, time step has to be smaller for brash ice as well. Therefore reduced frac values were tested.
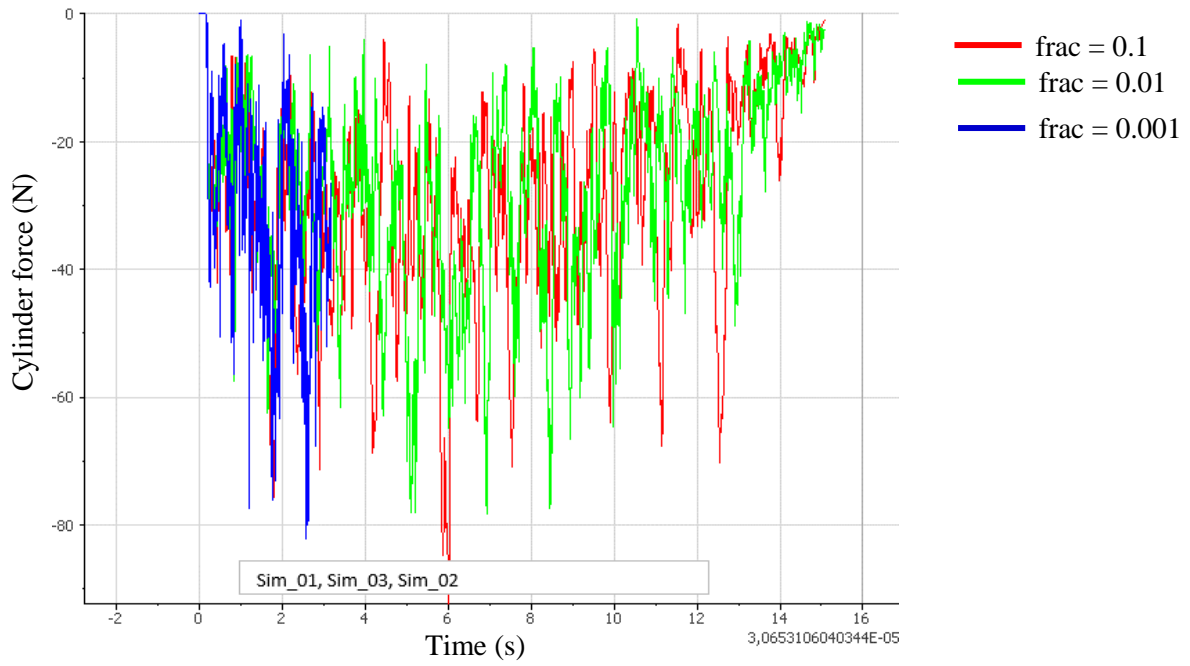
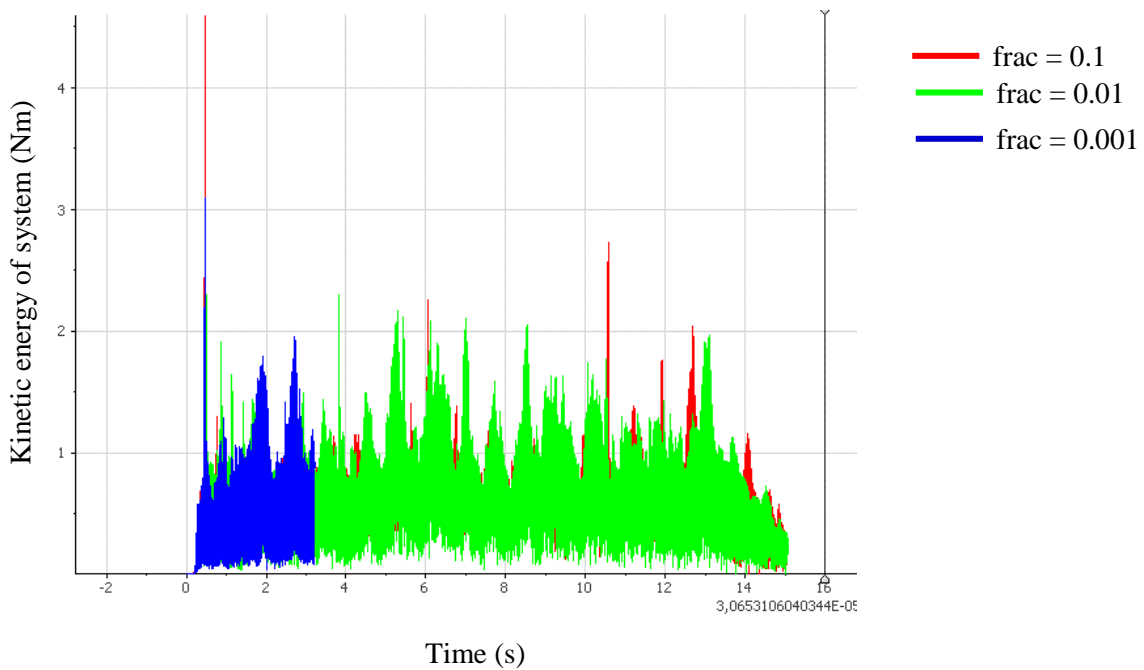*Figure 34: Influence of time step on cylinder force*

Figure 35: Influence of time step on total kinetic energy of the system

From the force on cylinder and kinetic energy of system, it can be observed that there is no significant difference for change of time step. Positive X direction of the domain is in to the cylinder movement direction. Therefore forces on cylinder has negative sign. Frac = 0.001 case has partial results, because the data logging has reached the limit of maximum rows supported
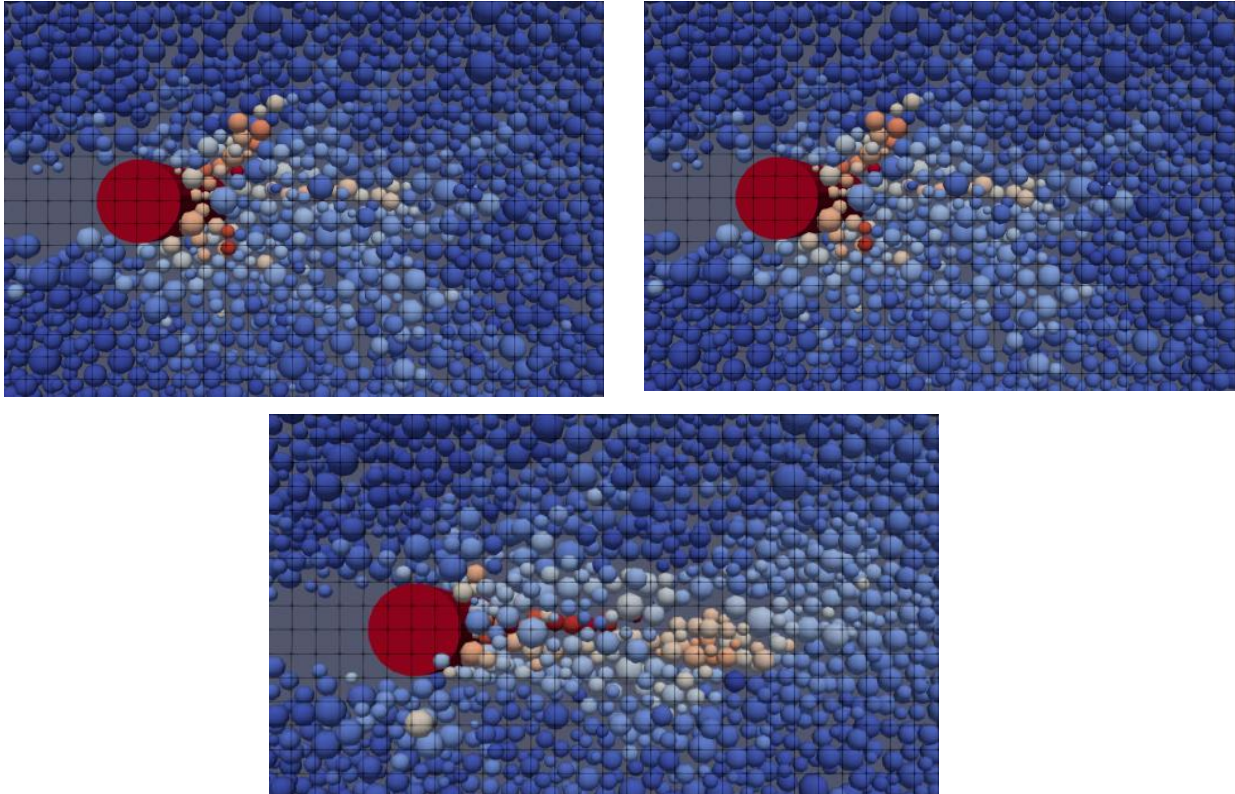

Figure 36: Effect of time step on far field-top left: frac=0.1, top right: frac=0.01, bottom: frac=0.001

by .csv file format. Far field behaviour of ice particles were also analysed.

Above figures, are taken at the same time instance in three simulations at around mid-point of the channel. The velocity distribution of particles and particle formation around cylinder are also not much different in three cases. Therefore it was concluded that frac 0.1 is the optimum value for brash ice simulation as well. Values larger than 0.1 were not considered as 0.1 was reference value from ridge breaking [14].

11.1.2 Influence of Young's Modulus of Ice

As explained in the force calculation section, contact forces are dependent on the young's modulus. Young's modulus acts as an internal parameter in simulation rather than an actual Young's modulus of ice. Therefore sensitivity of Young's modulus on simulation results is important. Reference value was taken from ridge ice simulation. Since actual Young's modulus of ice is higher than reference value, sensitivity was analysed for values higher than reference value.
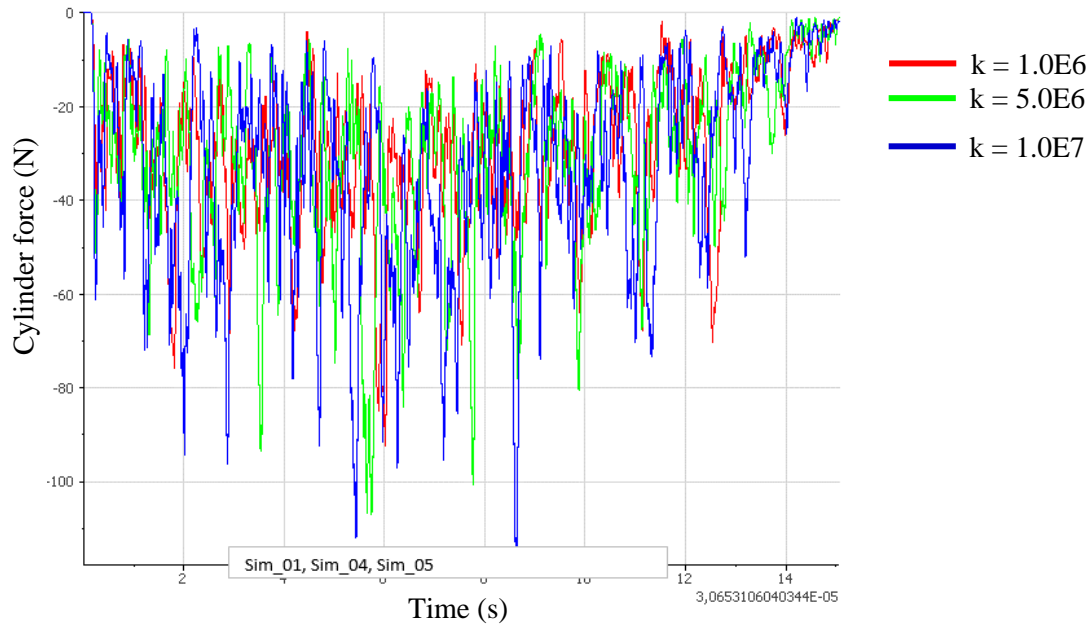
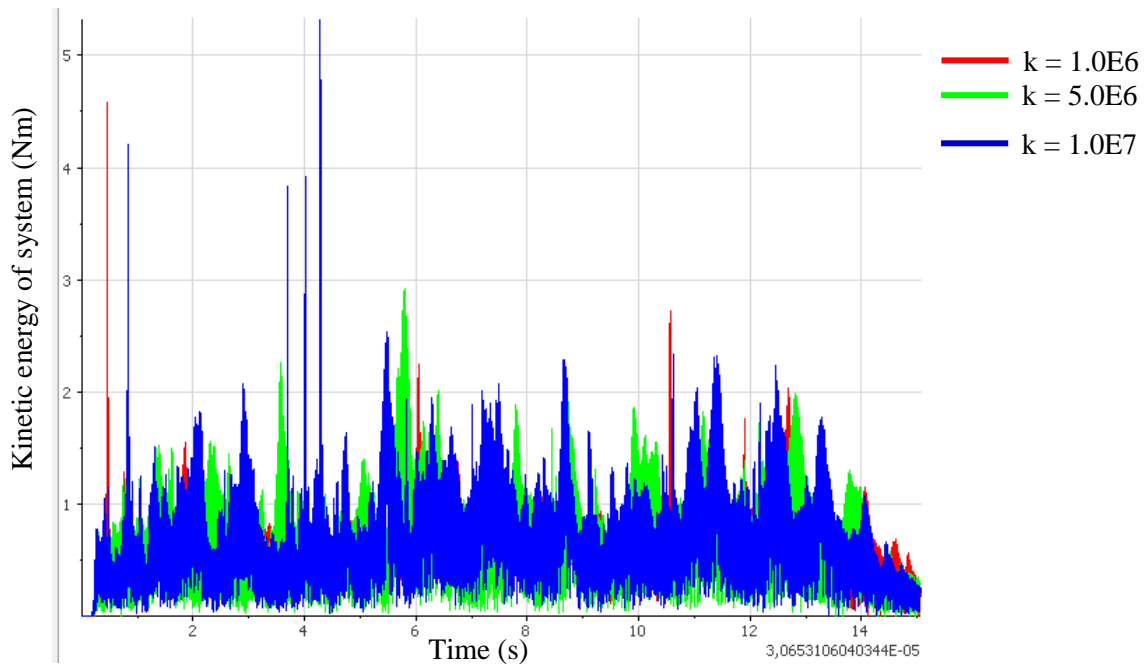*Figure 37: Influence of Young's modulus on cylinder force*

Figure 38: Influence of Young's modulus on total kinetic energy of the system

When comparing results of three simulations, it can be seen that there is no significant change of results. An increase of magnitudes of peaks can be seen in force results as Young's modulus increases. This is reasonable since normal contact forces increase with Young's modulus. However this increased normal forces are compensated by increased damping and friction.

Damping forces are proportional to the square root of Young's modulus. Cundall-Strack friction also has square root influence of tangential stiffness, which is dependent on Young's modulus. In addition change of Young's modules does not affect the time step since for the large structure simulations, time step is based on bending strength. Therefore although there is slight increase of kinetic energy in the system, it is not significant. Particle behaviour was also
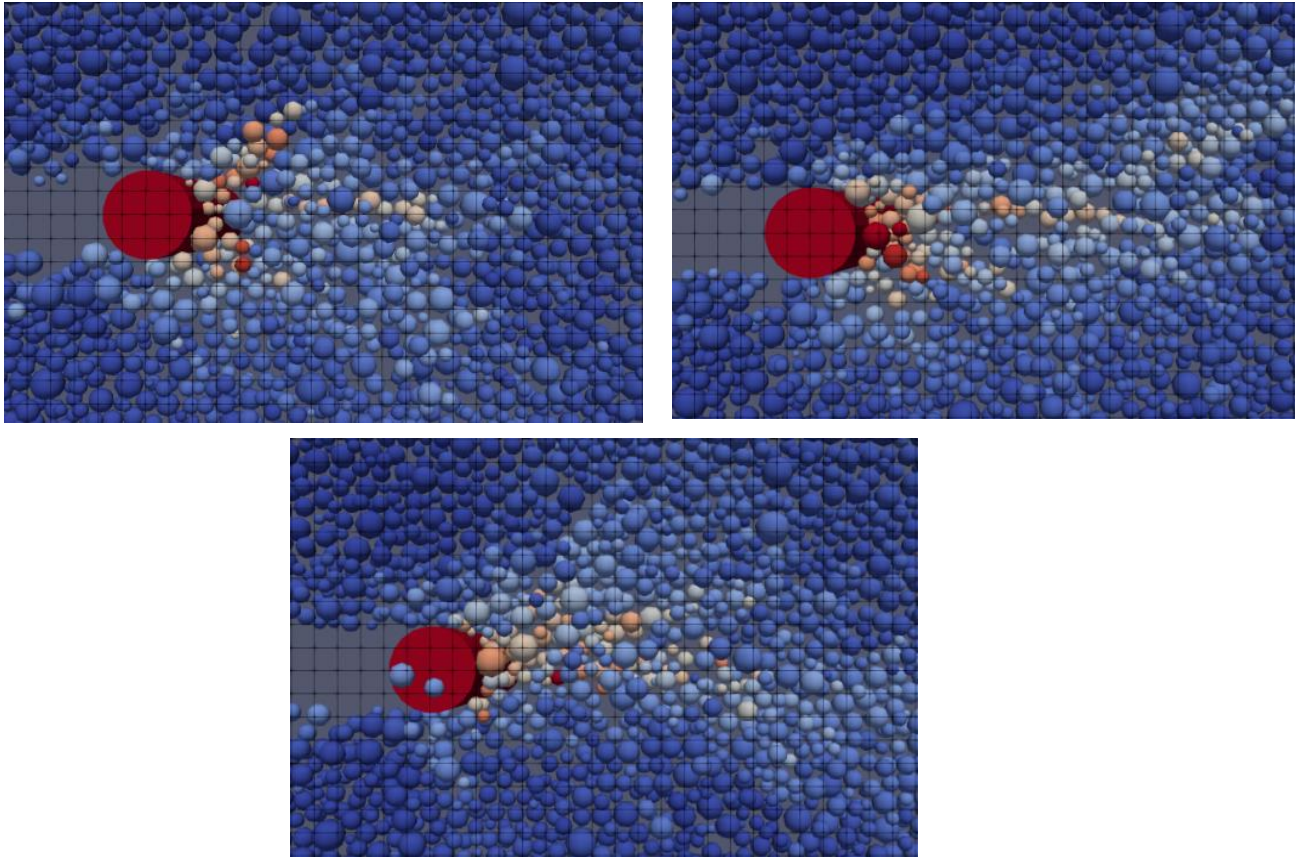

Figure 39: Effect of young's modulus on far field-top left: k=1.0e6, top right: k=5.0e6, bottom: k=1.0e7

studied, for all three cases. And there is no significant effect of Young's modulus on far field behaviour can be seen.

11.1.3 Influence of Friction Coefficient.

In case of spherical particle DEM simulations, friction has a great influence on the behavior of particles. Specially, on formation of particle in channel and around structure. Therefore different friction coefficient values were also tested. Reference value for friction coefficient was taken as one based on the literature. Literature suggests that brash ice has high friction angle, around 35° to 40° [15]. Therefore reference value was taken as one and descending values were tested.
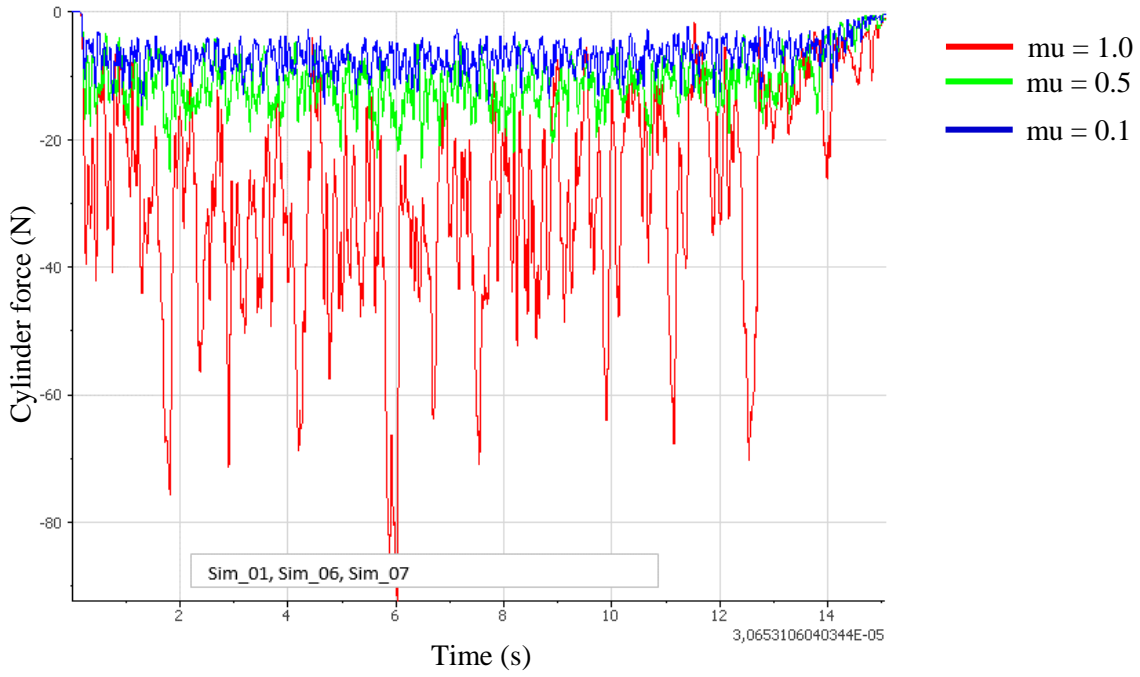
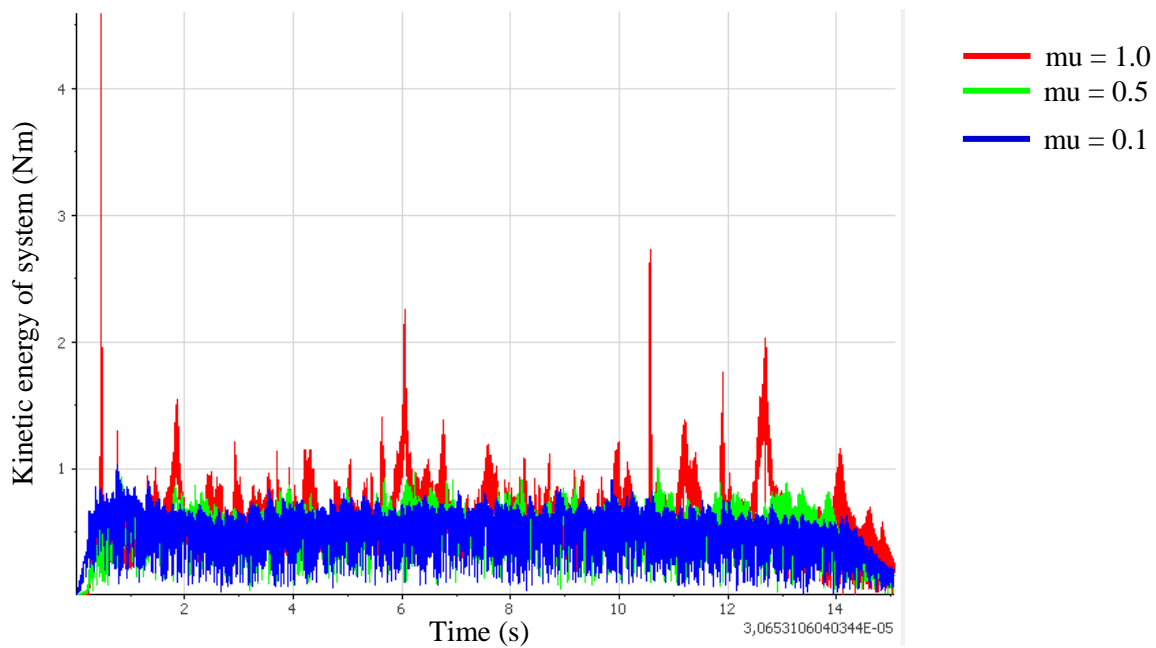*Figure 40: Influence of friction coefficient on cylinder force*

Figure 41: Influence of friction coefficient on total kinetic energy of the system

From the force graph it can be seen that horizontal force on cylinder is reducing drastically with the friction coefficient. Although it seems that there is a great, influence of friction coefficient on force, force on cylinder is reduced due to less number of contacts. This can be observed clearly in the far field analysis.
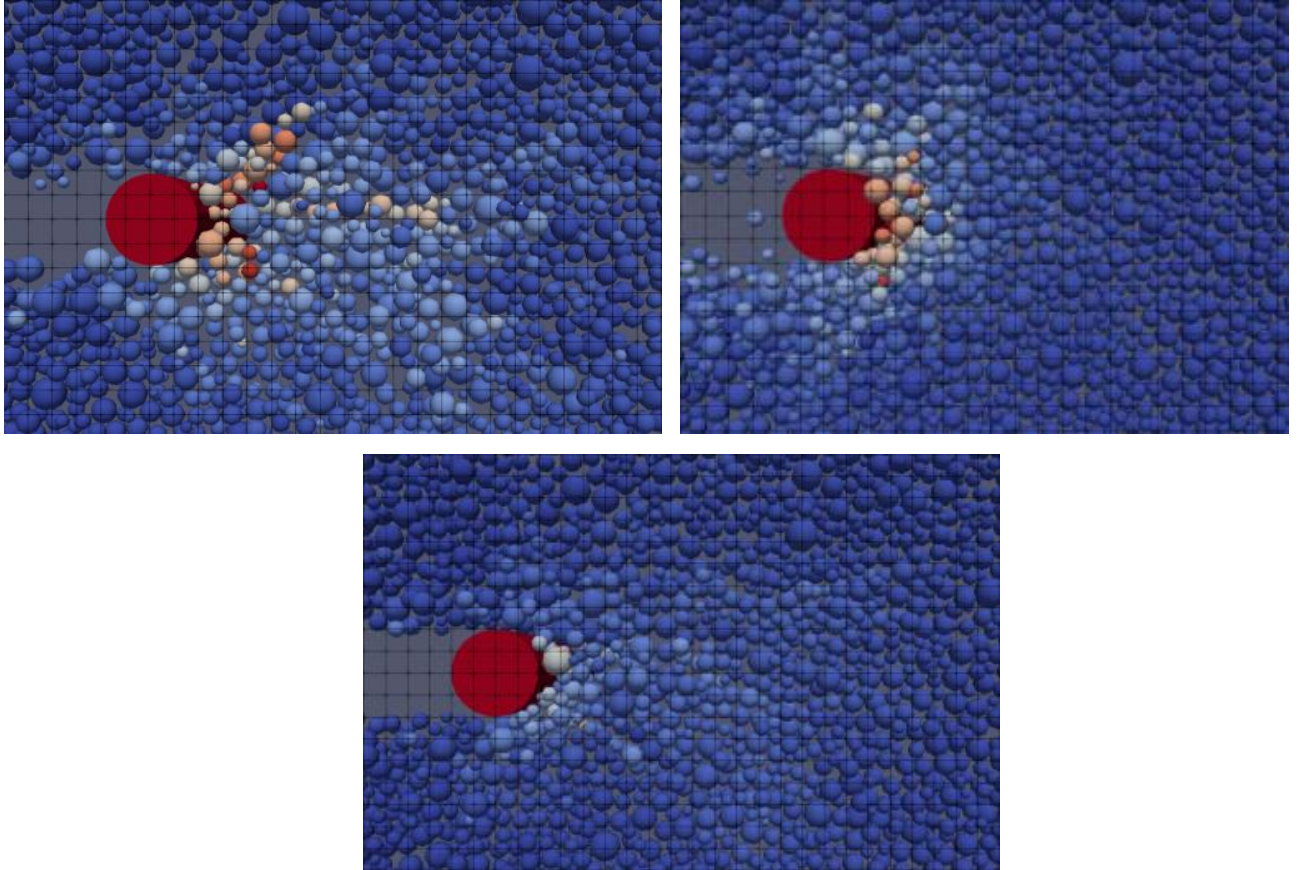

Figure 42: Effect of friction coefficient on far field-top left: mu=1.0, top right: mu=0.5, bottom: mu=0.1

From above three figures, it can be seen that effect of cylinder on ice channel is reduced as friction coefficient reduces. There are two reasons for this behavior. The first reason is, the channel flattens out by itself in low friction coefficients. As explained in the brash ice particles modeling section, friction is important to have the pilling behavior of spherical particles. When friction is low, channel thickness reduces over the time reducing force on cylinder as well. The next reason is the reduction of force transmission. In high friction coefficient case, force lines spread further into the ice. This means, cylinder is displacing more ice particles and higher forces occur. Although force transmission is due to both normal and friction forces, friction force seems to be more dominant in here. It is reasonable, since most of the far field particles are shearing due to movement of cylinder. In case of low friction, force transmission is less, and force on cylinder is less as well. This can be further seen in the kinetic energy graph as

well. When friction is decreased there is also a reduction of total kinetic energy of the system, which is due to less particle movements.

11.1.4 Influence of Cohesion Coefficient

As the final part, influence of cohesion coefficient of ice was studied. Cohesion coefficient was selected for study because, it is also an internal parameter of simulation, rather than the actual cohesion coefficient of ice. As explained in the force calculations, current version of cohesion force model is based on Young's modulus. Since the influence of Young's modulus for the results is less, cohesion coefficient was also varied to check the effects. The reference value was taken form DEM simulation of ridges. Since the reference value is significantly small, it was decided to increase the cohesion coefficient for analysis.
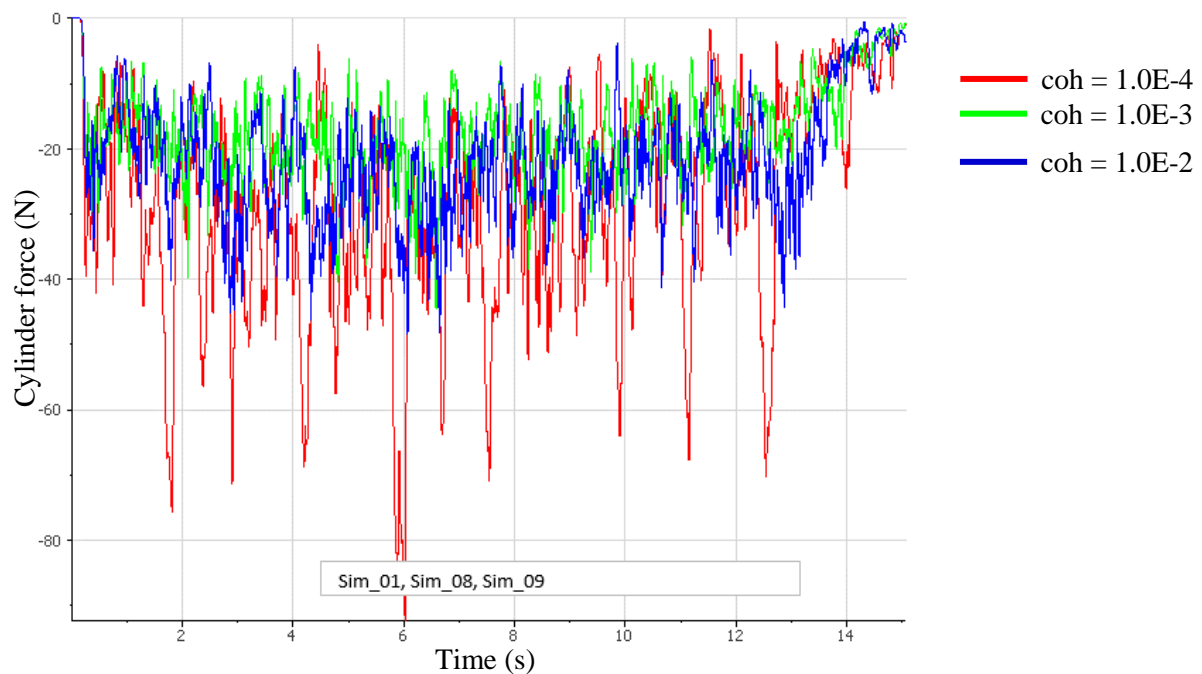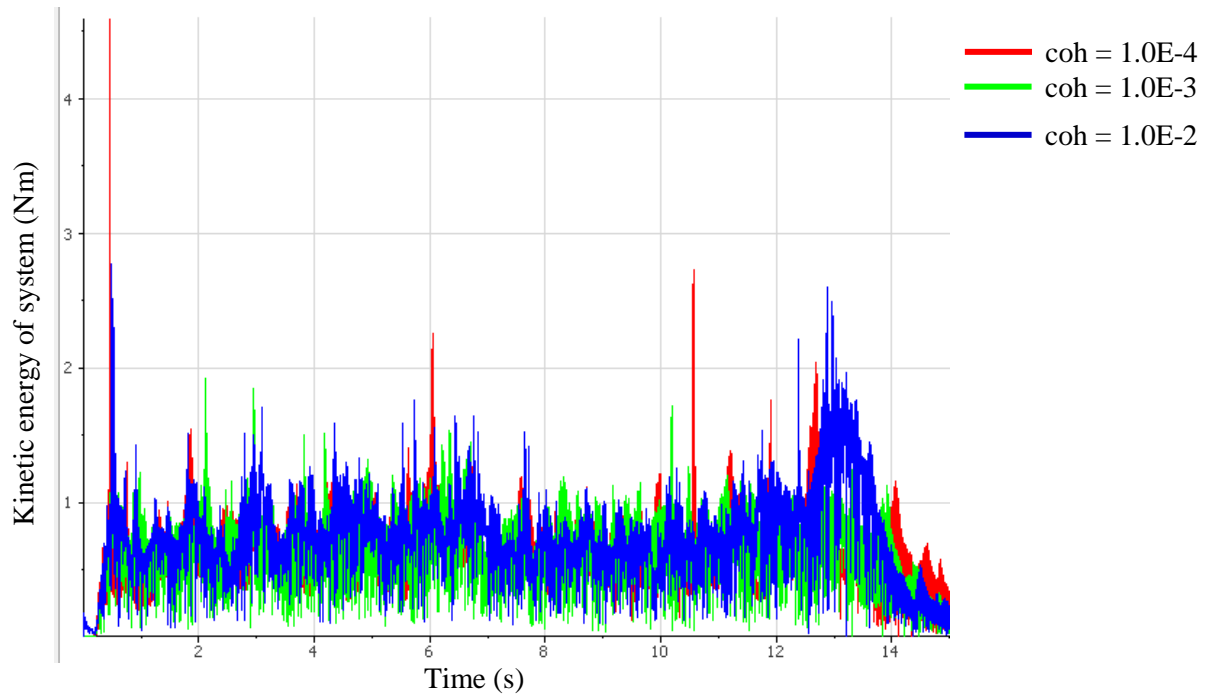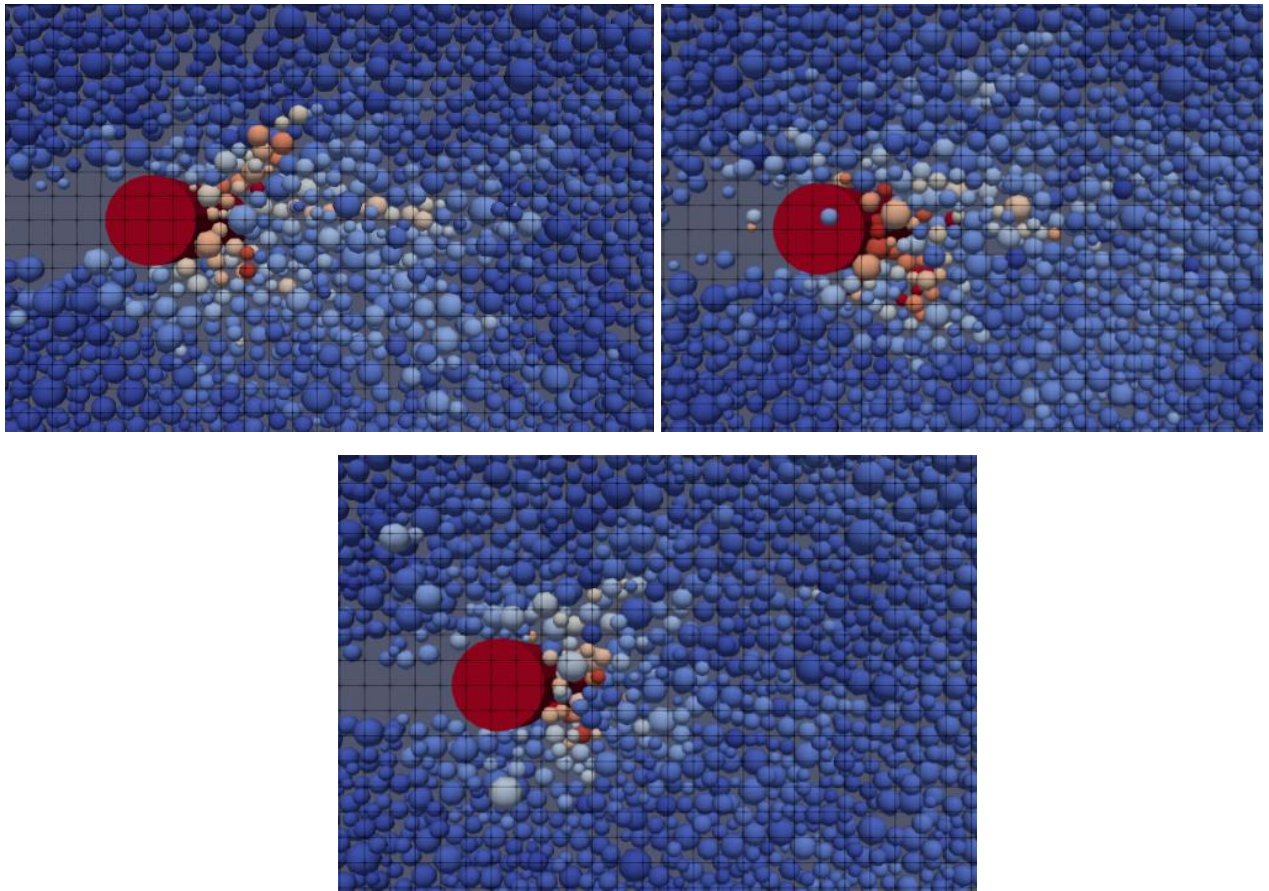
Figure 43: Influence of cohesion coefficient on cylinder force

Figure 44: Influence of cohesion coefficient on total kinetic energy of the system

From the force graph it can be seen that, force on cylinder has reduced as cohesion increases. Total kinetic energy of the system has decreased as well. Cohesion force is in opposite direction of normal reaction force. Therefore increase in cohesion, decreases the bouncing back velocity after the collision and reducing contact force. In addition total kinetic energy of the system is also reduced due to lesser bouncing back velocities and less movements of particles. This can be seen in far field analysis as well.

Figure 45: Influence of cohesion on far field-top left: coh=10e-4, top right: coh=1.0e-3, bottom: coh=1.0e-2

Although the cohesion effect seems to be significant in the simulation, it is very difficult to relate this cohesion coefficient to the actual cohesion forces between brash ice particles. Literature, suggests that cohesion between ice particles can vary a lot with external parameters such as temperature, impurities in water and static pressure [3]. Further sometimes, the cohesion can be effect of friction or vice versa.

11.2 Experimental Results

In the final stage simulation results were compared with an experimental results of a cylinder experiment in tank with similar test conditions. Experimental parameters and force results are given below.

Table 4: Experiment channel properties

Brash ice thickness	46.03 mm
Porosity	0.3304
Cylinder diameter	200 mm
Towing speed	0.74 m/s
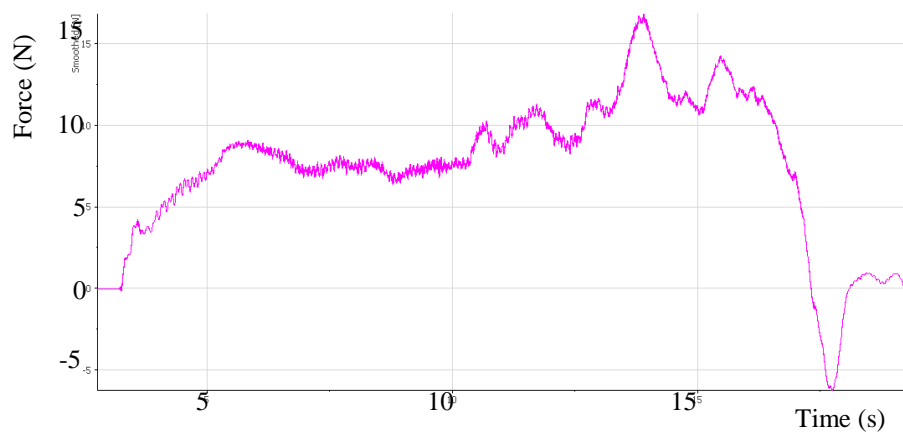
Figure 46: Cylinder force experimental results

When comparing the cylinder force in reference case simulation and experimental values, there is a significant difference. Simulation results are much higher than expected. Simulation parameters can be changed necessarily to match the results. From the sensitivity analysis, it can be seen that to decrease cylinder forces, friction coefficient has to be decreased or cohesion coefficient has to be increased. However reducing friction may flattens up the channel as explained in the sensitivity analysis. Therefore it is more acceptable to increase the cohesion. Nevertheless as explained in the sensitivity analysis, cohesion between ice particles should not be a significant factor upon ice load on cylinder. Therefore to identify further causes, underwater camera footage was also compared with the graphical output of the simulation.

Figure 47: Underwater view of cylinder experiment

Figure 48: Above water view of cylinder experiment

An important observation from underwater video is, there is less far field effect in the experiment when compared to simulation. Which is more similar to low friction coefficient case. To get more clear idea about ice particle behavior, another experiment with much lower carriage speed (0.19 m/s) was also analyzed. In this case the cylinder force was about half of the previous case results. Since dynamic friction is independent of speed, reduced speed should also have same magnitude of cylinder force, if friction is dominant. Therefore we can conclude that although friction has significant influence on results in the simulation, it is actually due to the reduced far field effect. And current friction model is not very good in modeling the exact far field effects. In the scale of cylinder simulation, channel is very large compared to cylinder. Therefore in the simulation, influence of far field effect on forces are higher than it should be. However in the case of ship model test, channel width is twice the ship breadth and particle

movement in the channel is much higher than cylinder experiment. Therefore the effect of the far field behavior should be less and better results can be expected. Considering all of the above factors, following parameters were selected as optimum values for ship model simulation.

Table 5: Final values from sensitivity analysis

frac	0.1
Youngs Modulus	1.0×10^6 N/m^2
Friction Coefficient	1.0
Cohesion Coefficient	1.0×10^{-4}

In conclusion, the cylinder experiment simulation is very helpful to identify the effects of different parameters on simulation results. However, results cannot be compared to actual cylinder experiment due to small scale of the simulation. As explained earlier, cylinder experiment simulation is only a reference and can be used to compare different channel properties in simulation environment.

Part IV: Ship Model Test Simulation

12 Simulation of Ice Class Tanker

As the final part of the thesis, a ship model test simulation was carried out. A model of ice class tanker which has been already tested in the ice tank was used. A tanker was selected because they are the most frequent brash ice going ships. Simulation was set up identical to the ice tank model test, so that results can be directly compared. As the first step, ice channel was generated according to the specifications.

Figure 49: Brash ice model test in ice tank

12.1   Generation of Ice Channel

Ice channel specifications are defined by the class society, according to the ice class notations. Ship model in the tank was tested for Ice Class 1A and 1B. Therefore two channels were generated according to the specifications of 1A and 1B.

Table 6: Channel Parameters

|	**Ship Data**	**Model Data**
Channel Length	749.85 m	23.43 m
Channel Width	88 m	2.75 m
Brash Ice Thickness(1B)	1.416 m	0.0442 m
Porosity (1B)	37.02%	37.02%
Brash Ice Thickness(1A)	1.616 m	0.0505 m
Porosity (1A)	25.71%	25.71%

Ice thickness and porosity data are from the corrected results of model experiment. They were converted to model scale again for the simulation. As per the standards, channel width is twice the ship breadth. Channel has to be sufficiently long enough so that ship can come to equilibrium at self-propulsion point. Therefore channel length was taken as three times ship length. Two ice channels were generated with above model data parameters as input. Simulation parameters were kept as values obtained from sensitivity analysis.

Photographs of ice channel in the tank was taken for a 1B channel with similar parameters. These photographs were used to compare the channel in simulation. Particle size and distribution are compared. Although particles dimensions in the ice tank are little larger than the simulation, it is compensated by the thickness. Ice sheet used to make the channel is about 23.5 mm thick while in simulation particles are spherical. Therefore mass of the particles in tank and simulation, can be taken as in same order.
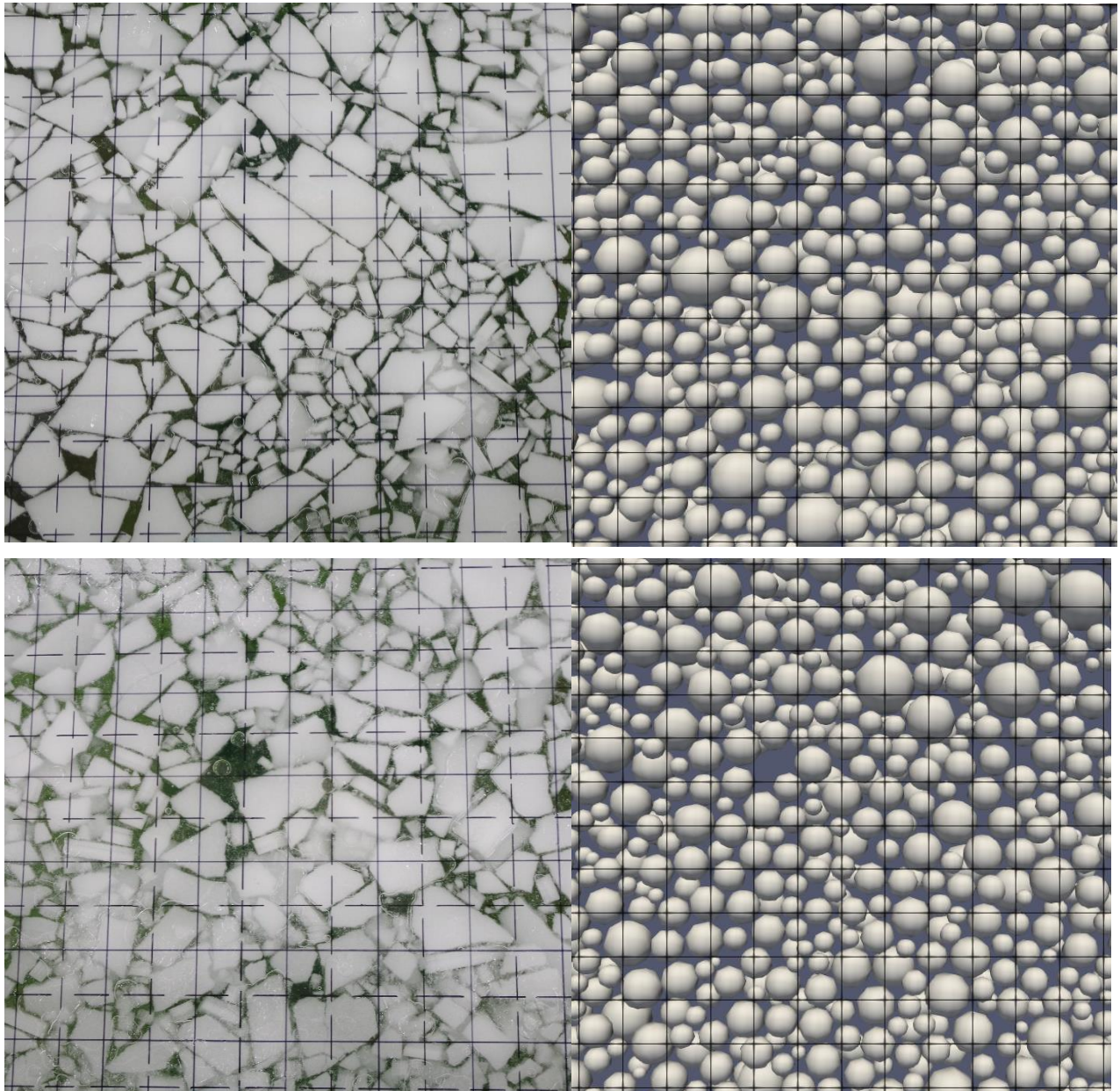
Figure 50: Comparison of channel 1B in ice tank and simulation – 50×50 mm grid

In addition channel thickness was also checked. Channel thickness of generated channel in the simulation is higher than the ice tank. However packing of ice particles in simulation is much looser than the tank. Therefore volume of ice in the simulation is similar to tank.
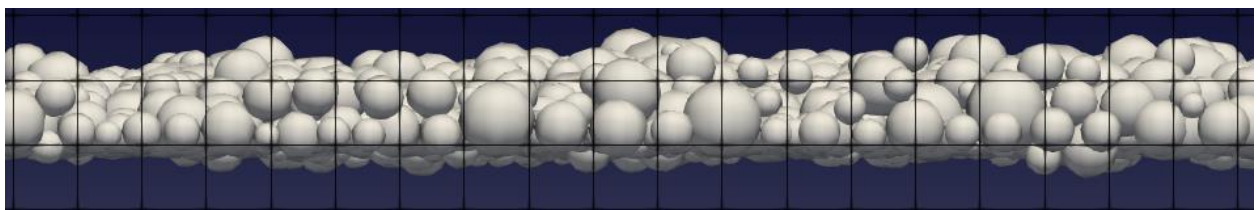
Figure 51: Channel 1B thickness– 50×50 mm grid

To confirm this total volume of ice particles in the simulation was calculated and compared with channel properties.

Table 7: Ice volume comparison

Simulation	1.9068 m^3
Ice Tank	1.8846 m^3

Channel 1B is consist of 68208 ice elements which is very large amount for this kind of simulation.

12.2 Ship Model Preparation

Selected tanker has following basic dimensions. Presented dimension values are rounded off for confidentiality purpose. However exact values were used for the simulations.

Table 8: Basic dimensions of the ship

	Ship Data	**Model Data**
Model Scale	-	1/32
LOA	250.0 m	7.81 m
Breadth	44.0 m	1.36 m
FWD Draft UIWL (Loaded)	15.9 m	0.50 m
AFT Draft UIWL (Loaded)	15.9 m	0.50 m
DISP UIWL (Loaded)	133900 m^3	4.08 m^3
FWD Draft LIWL (Ballast)	5.55 m	0.17 m
AFT Draft LIWL (Ballast)	8.57 m	0.27 m
DISP LIWL (Ballast)	53900 m^3	1.65 m^3
Speed	2.57 m/s (5 knots)	0.4547 m/s

The selected hull form has non-convex shapes in the bulbous bow and skeg. As explained in the part II ship model has to be in convex geometries. Therefore model was divided in to twenty convex sub-elements. A special attention was given to sub-elements along the water line so that ice particles will be in contact with less number of structure elements. Relatively thin elements were arranged along the water line so that, there would be less number of checks in contact detection algorithm. Hull form was received as IGES file format with rectangular surfaces. Rhinoceros was used to generate triangular surface mesh. Then .obj file was obtained for each sub-element.
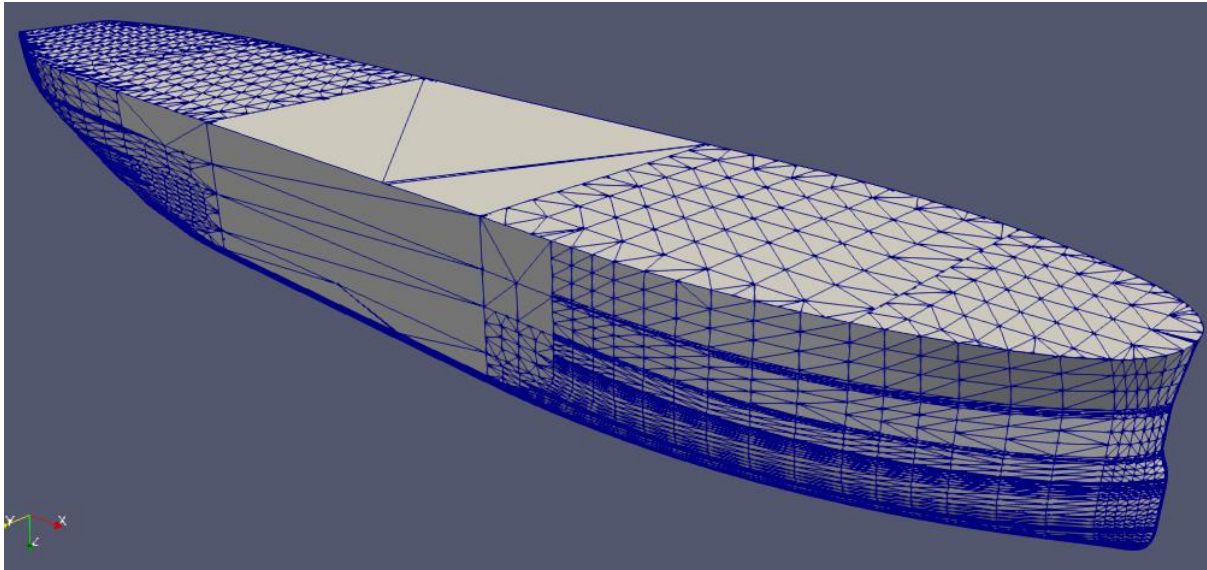
Figure 52: Ship mesh

Propeller characteristics of the HSVA's stock propeller used in the towing tank experiment was used in the simulation as well.

Table 9: Propeller Characteristics

Diameter	0.2442 m
Pitch/Diameter	1.1140
RPS	10
No of blades	4
Wake fraction	0.2
Thrust deduction factor	0.1170

12.3 Simulation Results

Simulation was run for Channel B1, full load condition and results were obtained. 2.7 GHz, eight core cluster was used, and simulation was run for about two weeks. In the end of simulation, vessel came to a still since the installed propeller power was not sufficient. Ice resistance is higher than expected, and propeller power has to be increased in order to keep the simulation running further. However further simulations could not be run due to the limited time frame of the master thesis. Results of the simulation are presented below.
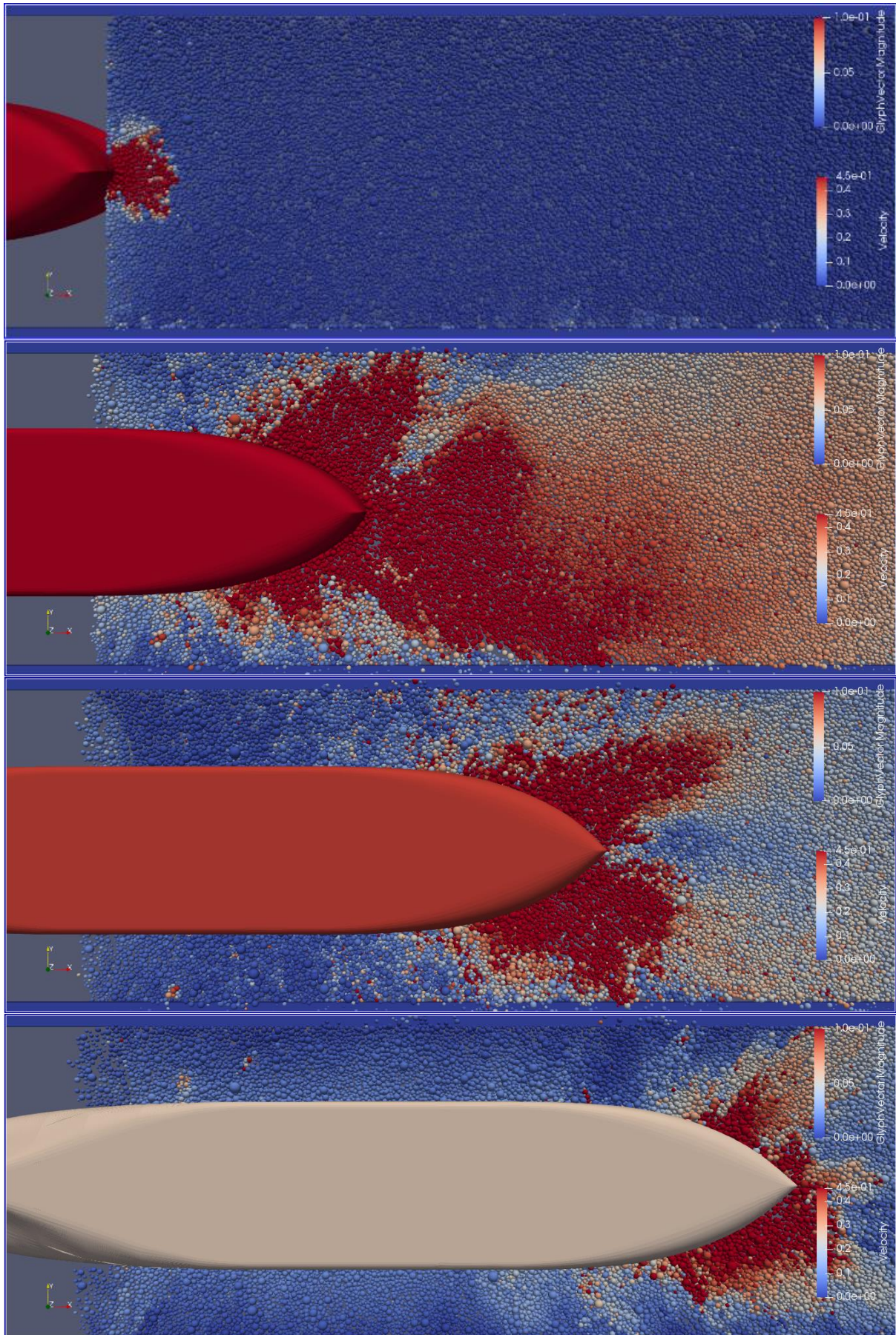
Figure 53: Ship passing through channel 1B – (legend for ice particles is from 0.1 m/s to 0.0 m/s while for ship 0.48 m/s to 0.0 m/s.)

Figure 53 illustrate the ship passing through channel in 4.38 s time intervals. Color shading on elements represent the particle velocity. For ice elements legend is upper scale on figure from 0.1 m/s to 0.0 m/s while for ship legend is bottom scale 0.48 m/s to 0.0 m/s. From the figure it can be observed that ship speed decreases as ship goes in to channel and comes to still.
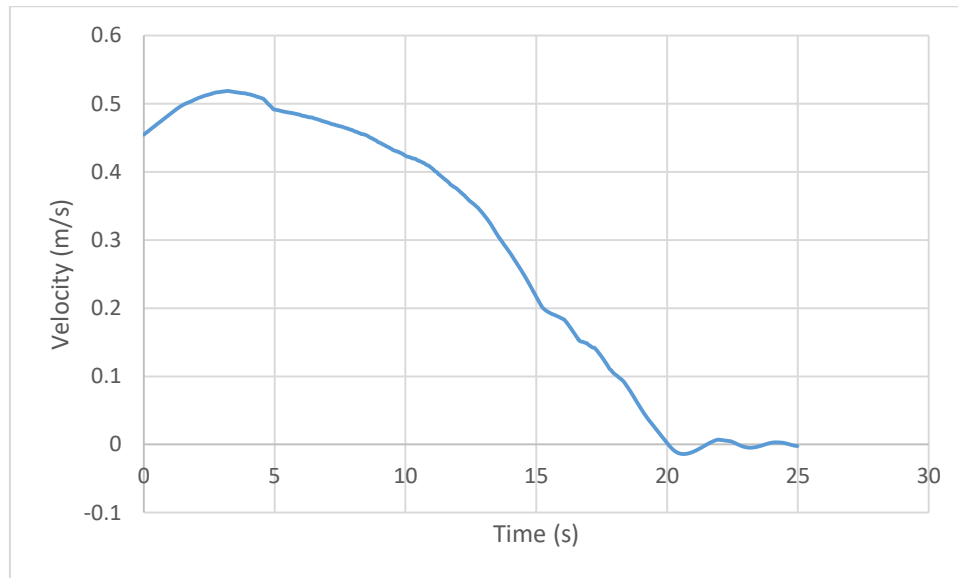

Figure 54: Ship velocity

In the beginning ship model is outside the channel and ice resistance is zero. Therefore ship accelerates towards the channel. As the ship enters in to the channel, ice resistance gradually increases. When ice resistance become larger than the available thrust at respective speed, ship gradually decelerates and comes to a still. Although the thrust is acting at the zero speed condition, high ice resistance prevents ships movement.
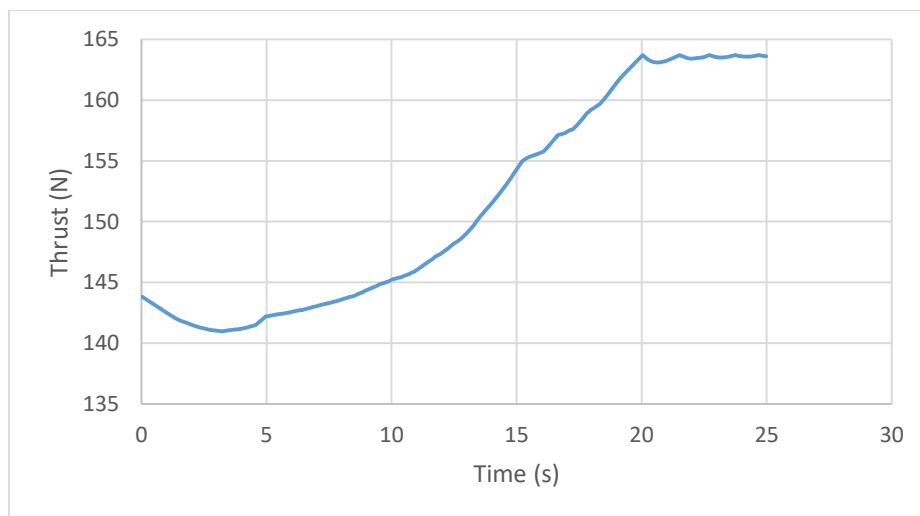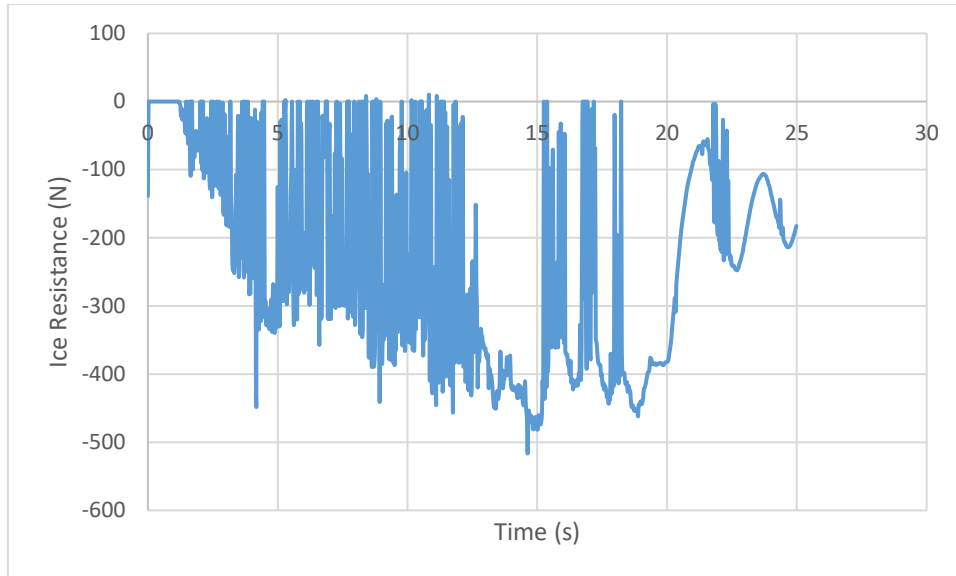

Figure 55: Thrust force

Figure 56: Added resistance due to ice

Additional simulations were run for Channel A1 with full load condition and Channel B1 with ballast condition. For A1 channel ice resistance was even higher than channel B1, and ship came to a still much faster.

12.4 Experimental Results

Since the simulation did not run as intended, numerical values of ice resistance was not compared. However to study the behavior of ice particles, and probable causes for high ice resistance in simulation, underwater video and graphical output of the simulation were compared for design speed 0.4547 m/s. Ice particle behavior near bow was compared for both loading conditions, because of high ice-structure interaction in this area.

In ship model simulation, ice particles near the hull has similar behavior compared with experimental results. Especially simulation was able to predict the ice particles movement near the bilge radius and flat bottom in ballast condition. However the far field movements of ice particles are much higher in simulation, as similar to results of cylinder experiment. Therefor it can be assumed that high ice resistance is due to deficiencies in the friction model in this case as well.
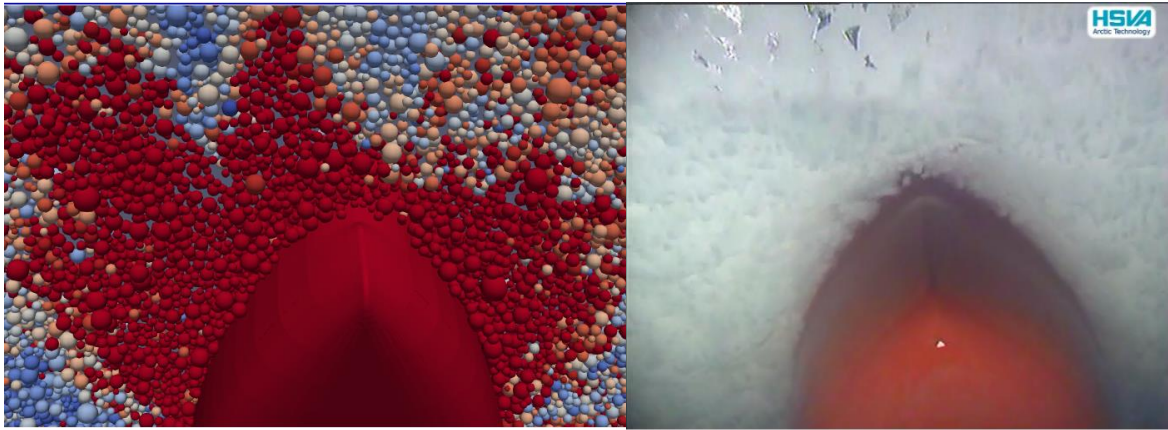
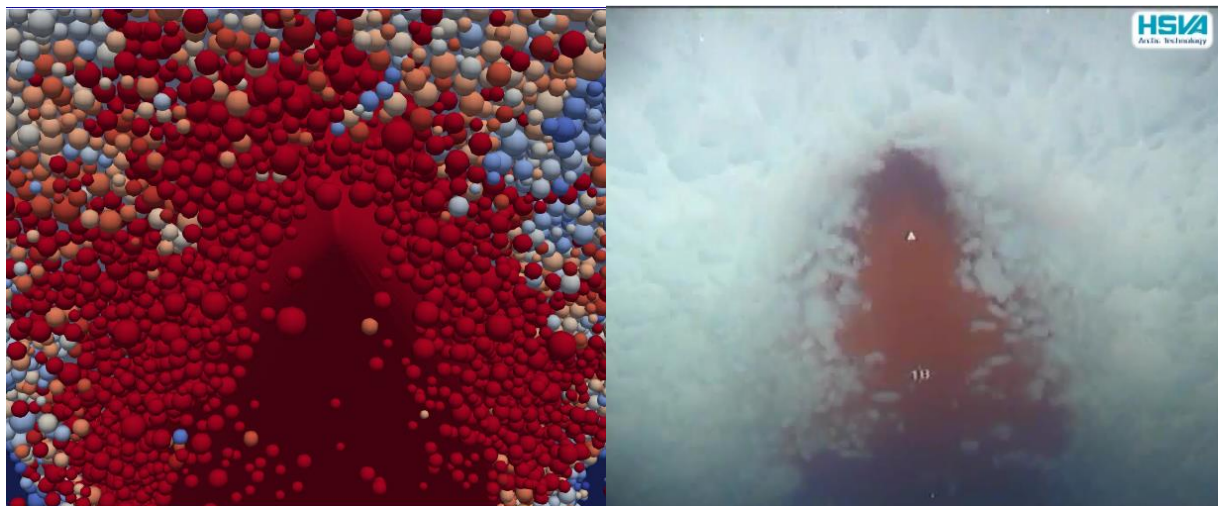*Figure 58: Ice Particle behavior near bow-front view (loaded condition)*
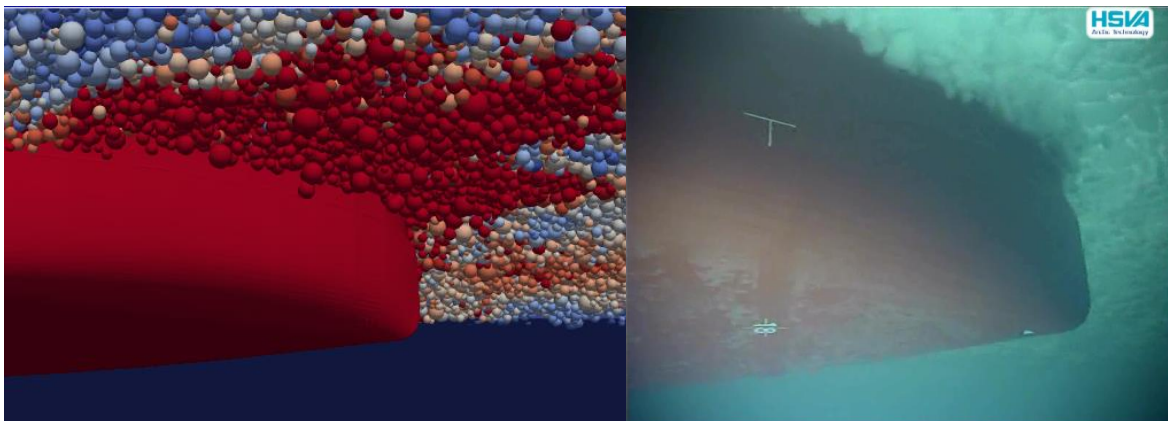
Figure 59: Ice Particle behavior near bow-side view (loaded condition)

Figure 57: Ice Particle behavior near bow-front view (ballast condition)
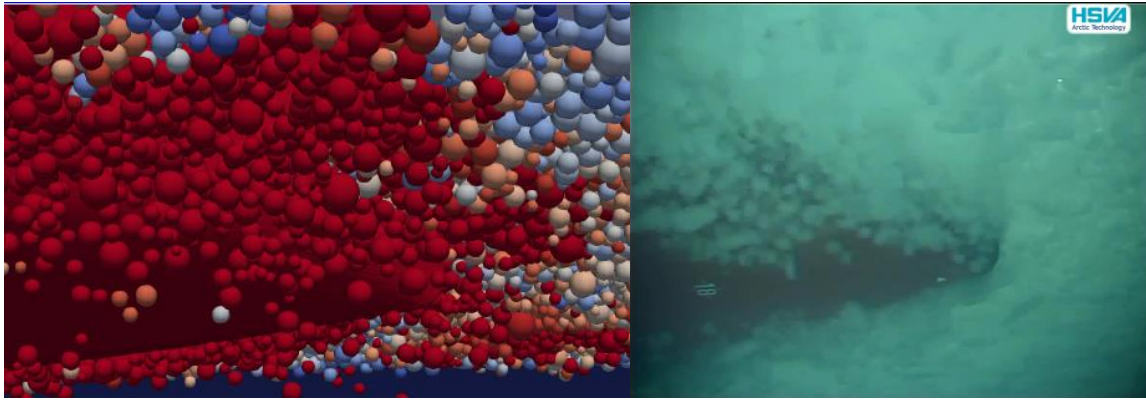
Figure 60: Ice Particle behavior near bow-side view (ballast condition)

Figure 57 to 60 illustrate a comparison between ice particle behavior near bow. This kind of qualitative validation can be very useful in design process as well. It allows for example to evaluate how much additional friction between ice pieces and the hull bottom (due to buoyancy forces of the ice) is to be expected. It is also useful to evaluate how much ice is likely to reach the propeller.

Conclusion and Future Prospects

13 Conclusion on Master Thesis Work

Objective of this master thesis was to develop a numerical tool capable of simulating brash ice model experiments. This task has been completed with a DEM tool and incorporated to HSVA's DEM tool for ridge breaking simulations. Different cases of cylinder experiment, were simulated and results were discussed. Further, simulation of a ship model was also carried out and results were compared with experimental values.

As the first conclusion by the results of the project, it can be seen that Discrete Element Method is a suitable tool to simulate ship-brash ice interaction. Brash ice particles can be modeled by discrete elements and their interaction with each other and structures can be analyzed using a DEM scheme. Ice load on ship and self-propulsion point of the ship can be obtained with the simulation. However since the tool is in initial development stage, numerical results have high margin of error. This is due to the simplified numerical model of ice-ice friction interactions. Time required to complete one simulation is also little bit higher than expected. The ship model simulation took about two weeks on a 2.7 GHz eight core computer.

When comparing the graphical output of the developed software, it can be seen that near field behavior of the ice particles is reasonable. This can be used to visualize the ice flow around the ship hull, which is a very significant design aspect. A possible case of analysis would be quantity of ice flowing under the hull, clogging of ice particles around appendages or excessive flowing of ice particles to the propeller. Ice particles flowing under the hull generates additional friction force on the vessel. In the current context these problems are identified by a model test in the later design stage where it requires major design modifications. However with the developed software, this can be done in very early stage saving lot of time and effort.

Therefore in conclusion although the numerical results have high margin of error, the present tool can be used to visualize ice particle behavior around structures. This will be helpful for designers in early design stage.

14 Future Prospects

Major technical difficulty of the current version of software is friction and damping model. As it was explained in the section five, software use Cundall-Strack Friction model since conventional Coulomb Friction model is difficult to implement in a numerical scheme. This is due to the two stage behavior of Coulomb Friction in dynamic and static conditions. Cundall-Strack method uses estimation of tangential force from previous time step to calculate friction. Therefore this method leads to a delay in tangential force relative to exact friction. Use of more advance friction model can be a solution to this problem [13]. In addition to friction force, tangential damping force model suggested in DEM also has some complications. Software tool tend to be unstable for some cases. Therefore current version of the software neglects the tangential damping forces. Force model for tangential damping has to be updated with a more realistic one in this case.

Current version of the software has developed using standard shape of mathematical formulas for force calculation and contact detection. However in a computer calculation some mathematical operations can be faster than other; as an example taking square of a function can be faster than taking the square root. Therefore expressions in the simulation can be rearranged mathematically, so that they run faster in a computer. In addition variable definitions can be changed as well. However this has to be done very carefully considering all the mathematical expressions in the simulation.

Implemented software tool is able to run on a computer cluster with Multi-Processing. However the existing version does not capable of parallel processing between multiple computers on a cluster. Processing of the tool is limited in a single computer on a cluster although there are more resources available. Hence implementing parallel computing features in the tool will make it much faster and efficient on a computer cluster.

Further introducing GPU accelerated computing can make the tool run faster even in a personal computer or workstation with a dedicated Graphical Processing Unit. GPUs are much faster than CPUs for parallel processing of small computations such as in the DEM code.

After addressing the potential problems identified in the scope of this thesis, developed tool can be very helpful in early stage design process to determine required installed power onboard. Correct estimation of required power will help to identify the most efficient hull form. In general optimization algorithms coupled with CFD codes are used in industry to automate the optimization process for non-ice class vessels. However in case of ice class vessels there is a lack of simulation tools to determine ice resistance for optimization. Therefore the developed tool can address the technological gap in industry for ship optimization and help to design more efficient ships in the future.

Acknowledgement

First of all, I would like to be grateful to Dr. Janou Hennig, Managing Director of The Hamburg Ship Model Basin and Dipl.-Ing. Nils Reimer, Head of Department Arctic Technology, for making the opportunity to perform internship and Master Thesis in The Hamburg Ship Model Basin.

Next, I would like to express my sincere gratitude to M.Sc. Quentin Hisette, for the continuous guidance, supervision and unconditional help, throughout the development of this Master Thesis. A special thanks goes to Prof. Robert Bronsart for the constructive comments and suggestions on results and thesis report. At last but not least, I would like to thank all the staff members of Arctic Technology Department for their tremendous support during experiments.

This thesis was developed in the frame of the European Master Course in Integrated Advanced Ship Design named EMSHIP for European Education in Advanced Ship Design, Ref.: 159652-1-2009-1-BE-ERA MUNDUS-EMMC.

Malith Prasanna

References

[1]   A. Council, "Arctic Marine Shipping Assessment 2009 Report," Arctic Council, 2009.

[2]   Jens-Holger Hellmann, Karl-Heinz Rupp, Walter L. Kuehnlein, "MODEL TESTS IN BRASH ICE CHANNELS," in *Offshore Mechanics and Arctic Engineering*, Greece, 2005.

[3]   H.-P. H. Robert Ettema, "Ice Formation in Frequently Transited Navigation Channels," US Army Corps of Engineers, 1990.

[4]   P. Greisman, "Brash Ice Behavior," United States Coast Guard, Research and Development Center, Groton, Conneticut, 1981.

[5]   Michael Lau, Karl P. Lawrence,Leo Rothenburg, "Discrete Element Analysis of Ice Loads on Ships and Structures," in *Narional Research Council Canada*, 2011.

[6]   JI Shunying, LI Zilin, LI Chunhua, SHANG Jie, "Discrete elementmodeling of ice loads on ship hulls in broken ice fields," in *The Chinese Society of Oceanography and Springer-Verlag*, Berlin, 2012.

[7]   Arto Sorsimo, Tapio Nyman, Jaakko Heinonen, "Ship-ice interaction in a channel," VTT Technical Research Centre, Espoo, 2014.

[8]   Akihisa Konno, Akihiro Nakane, Satoshi Kanamori, "VALIDATION OF NUMERICAL ESTIMATION OF BRASH ICE CHANNEL RESISTANCE WITH MODEL TEST," in *Port and Ocean Engineering under Arctic Conditions*, Espoo, 2013.

[9]   I. M. Cabrera, "Smoothed particle hydrodynamics modeling of brash ice," niversity of Rostock, Rostock, 2017.

[10] Quentin Hisette, Aleksei Alekseev, Johannes Seidel, "Discrete Element Simulation of Ship Breaking Through Ice Ridges," in *International Ocean and Polar Engineering Conference*, San Fransisco, 2017.

[11] "Simulation-Based Engineering Lab: High-Performance Computing for Applications in Engineering," 2011. [Online]. Available: http://sbel.wisc.edu/Courses/ME964/2011/Lectures/lecture0224.pdf

[12] C. Ericson, Real-Time Collision Detection, Burlington, MA: Morgan Kaufmann, 2004.

[13] H.-G. Matuttis, Discrete Element Method: Simulation of Non-Spherical Particles for Granular and Multi-Body Systems, Singapore: John Wiley & Sons, 2014.

[14] A. Alekseev, "Numerical Simulation of Ice Ridge Breaking," University of Rostock, Rostock, 2016.

[15] M. Mellor, "SHIP RESISTANCE IN THICK BRASH ICE," *Cold Regions Science and Technology,* 1980.

[16] J. Burkardt, "RANLIB General Random Number Generators," 31 March 2013. [Online]. Available: https://people.sc.fsu.edu/~jburkardt/f_src/ranlib/ranlib.html.

[17] J. Seidel, "Numerical prediction of the keel resistance of first-year pressure ice ridges on offshore structures," Technical University of Berlin, Berlin, 2016.

[18] "Two spheres intersection," AmBrSoft, 20 February 2017. [Online]. Available: http://www.ambrsoft.com/TrigoCalc/Sphere/TwoSpheres/Intersection.htm.

[19] C. Ericson, "Optimizing a sphere-triangle intersection test," 30 December 2010. [Online]. Available: http://realtimecollisiondetection.net/blog/?p=103.

[20] AmBrSoft, "Intersection of a Line and a Sphere," AMBRweb, 18 02 2016. [Online]. Available: http://www.ambrsoft.com/TrigoCalc/Sphere/SpherLineIntersection_.htm.

[21] Severin Strobla, Arno Formellab, Thorsten Pöschela, "Exact calculation of the overlap volume of spheres and mesh elements," *Journal of Computational Physics,* 2016.

[22] T. H. S. M. B. Arctic Technology Department, "Brash Ice Model Tests," Hamburg, 2017.